Aus der Klinik für Neurologie
der Medizinischen Fakultät Charité- Universitätsmedizin Berlin

DISSERTATION

´´Investigation of early histopathological changes in rodent models of Alzheimer's Disease, Parkinson's Disease and CADASIL: Brain magnet resonance elastography for early disease detection and staging correlated to histopathology and analysis of neurogenesis and cell survival``

zur Erlangung des akademischen Grades
Doctor medicinae (Dr. med.)

vorgelegt der Medizinischen Fakultät
Charité-Universitätsmedizin Berlin

von

Tonia Laura Munder

aus Weingarten

Datum der Promotion: 16.6.2018

List of abbreviations

Aβ	β Amyloid
AD	Alzheimer's disease
BrdU	5-bromo-2-deoxyuridine
BW	Body weight
CADASIL	Cerebral autosomal dominant arteriopathy with subcortical infarcts and leukoencephalopathy
cm	Centimeter
CTR	Control
DAB	3,3`-Diaminobenzidine
DAPI	4′6-diamidino-2-phenylindole
DG	Dentate gyrus
DNA	Deoxyribonucleic acid
ENR	Enriched environment
FoV	Field of view
g	Gram
H202	Hydrogen peroxide
HCL	Hydrochloric acid
Hz	Hertz
Iba-1	Ionized calcium-binding adaptor molecule 1
i.p.	intraperitoneal
kPa	Kilopascal
m	Meter
MB	Midbrain
mg	Miligram
mm	Milimeter
MPTP	1-methyl-4-phenyl-1,2,3,6-tetrahydropyridine
MRE	Magnet resonance elastography
MRI	Magnet resonance imaging
ms	Milisecond
MSG	Motion sensitizing gradient
mT	Militesla
NaCl	Sodiumchloride
NeuN	Neuronal nuclei
NiCl	Nickelchloride
PBS	Phosphate-buffered saline
PD	Parkinson's disease
PFA	Paraformaldehyde
RM	Repeated measures
ROI	Region of interest
rpm	Rounds per minute
RUN	Running wheel
s	Second
S.E.M.	Standard error of the mean
SGZ	Subgranular zone
SN	Substantia nigra
STD	Standard environment
T	Tesla
TH	Tyrosinhydroxylase
WT	Wild type

Abstract (English)

Alzheimer's disease (AD), Parkinson's disease (PD) and Cerebral Autosomal Dominant Arteriopathy with Subcortical Infarcts and Leukoencephalopathy (CADASIL) show particular neuropathologies prior to cognitive symptoms. Extra- and intracellular amyloid β accumulation (AD), loss of dopaminergic neurons (PD) and vascular and white matter degeneration (CADASIL) are hallmarks disrupting brain homeostasis and observable in hippocampus, substantia nigra and cortex. Methods sensitive enough to detect relevant early histological alterations are needed to enable early interventions. Magnetic resonance elastography (MRE) is a promising method for capturing biomechanical changes of local alterations in tissue viscoelasticity. We investigated how MRE can be used for correlation of viscoelasticity with histology as step towards using MRE for early diagnosis and/or disease staging. Also we studied effects of counteracting mechanisms as varied physical activities and environments.

In study 1 we investigated the APP23 mouse model of AD under standard (STD) and enriched (ENR) living conditions at three early disease stages and correlated MRE data to histological changes. The biomechanical response of MRE to brain areas affected in the 1-methyl-4-phenyl-1,2,3,6-tetrahydropyridin hydrochloride (MPTP) mouse model of PD correlated to histopathology was subject of study 2. In study 3 mice overexpressing wild type Notch3 ($TgN3^{WT}$) and mice with a CADASIL mutation were exposed to ENR, a running wheel (RUN) and STD to further elucidate the mutations effect on neurogenesis and cell survival at early disease stages. MRE may also be a candidate for future early diagnosing and staging in CADASIL when early disease features are better understood.

In study 1 viscosity (cellular network) and cell numbers in the hippocampus decrease with disease progression in APP23 mice and ENR is insufficient to counteract both processes. Hippocampal elasticity (cell density) is lower in young APP23 mice but increases as intracellular amyloid β deposits transiently rise with age. In study 2 we observed a decrease of viscosity and elasticity in the substantia nigra correlating to neurodegeneration of MPTP treated mice. Study 3 showed that neurogenic stimulation by RUN and ENR is impaired in both $TgN3^{WT}$ and CADASIL mice due to micromilieu changes.

In summary with MRE alterations in viscoelasticity in small brain areas are detectable and relatable to early histopathological changes on a cellular level in AD and PD. ENR could not counteract the cell loss and change in viscosity in APP23 mice, nor could neurogenesis be stimulated by RUN or ENR in $TgN3^{WT}$ and CADASIL mice.

Abstract (German)

Morbus Alzheimer (AD), Morbus Parkinson (PD) und Cerebral Autosomal dominante Arteriopathie mit subkortikalen Infarkten und Leukoenzephalopathie (CADASIL) zeigen präsymptomal spezifische Histopathologien. Extra- und intrazelluläre Amyloid-β-Akkumulation (AD), Verlust von dopaminergen Neuronen (PD) und vaskuläre und weiße Substanz Degeneration (CADASIL) stören die Gehirnhomöostase im Hippocampus, in Substantia Nigra und im Kortex. Von besonderem Interesse sind Methoden, die relevante frühhistologische Veränderungen erkennen, um frühzeitig zu intervenieren. Magnetresonanz-Elastographie (MRE) ist eine vielversprechende Methode in der Erfassung lokaler biomechanischer Veränderungen der Gewebe-Viskoelastizität. Viskoelastizitätsparameter wurden mit Histopathologien korreliert, um die Eignung von MRE für die Früherkennung und /oder Stadieneinteilung zu analysieren. Auch wurden Effekte von körperlicher Betätigung und einer reizreichen Umgebung untersucht. In Studie 1 wurde das APP23-Mausmodell für AD unter Standard (STD) und reizvolleren (ENR) Lebensbedingungen in drei frühen Krankheitsstadien untersucht und MRE-Daten zu histologischen Veränderungen korreliert. In Studie 2 wurde die biomechanische Reaktion von MRE auf Hirnareale, die im 1-Methyl-4-phenyl-1,2,3,6-tetrahydropyridin-hydrochlorid (MPTP)-Mausmodell von PD betroffen sind untersucht und ebenfalls mit histologischen Veränderungen korreliert. In Studie 3 wurden Mäuse mit Wildtyp Notch3 Überexprimierung ($TgN3^{WT}$) und Mäuse mit einer CADASIL-Mutation ENR, einem Laufrad (RUN) und STD ausgesetzt, um den Einfluss auf Neurogenese und des Zellüberlebens bei frühen Krankheitsstadien zu ermitteln. MRE kann künftig auch hier nützlich für die Früherkennung/Stadieneinteilung sein, wenn frühe Krankheitsmerkmale besser erfasst sind. In Studie 1 nehmen die Viskosität (zelluläres Netzwerk) und Zellzahlen im Krankheitsverlauf der APP23 Mäuse im Hippocampus ab und ENR ist unzureichend diesen Prozessen entgegenzuwirken. Die hippocampale Elastizität (Zelldichte) ist bei jungen APP23-Mäusen geringer, nimmt aber mit dem vorübergehenden Anstieg der intrazellulären Amyloid-β-Ablagerungen zu. In Studie 2 beobachten wir eine Abnahme der Viskosität und der Elastizität in der Substantia Nigra, die mit der Neurodegeneration von mit MPTP behandelten Mäusen korreliert. Studie 3 zeigte, dass Neurogenese durch RUN und ENR sowohl bei $TgN3^{WT}$ als auch bei CADASIL-Mäusen aufgrund von Veränderungen des Mikromilieus beeinträchtigt wird. Zusammenfassend kann man mit der MRE Veränderungen der Viskoelastizität in kleinen Hirnarealen nachweisen und mit frühen histopathologischen Veränderungen auf zellulärer Ebene korrelieren. ENR konnte dem Zellverlust und der Viskositätsänderung bei APP23-Mäusen nicht entgegenwirken, noch konnte die Neurogenese durch RUN oder ENR in $TgN3^{WT}$ und bei CADASIL-Mäusen stimuliert werden.

1. Introduction

Higher life expectancy, a lifestyle with limited physical activity and a high fat diet are characteristics of developed societies. Increased occurrence of neurodegenerative diseases like Alzheimer's- (AD) and Parkinson's Disease (PD) (1-3) is observed. In Cerebral Autosomal Dominant Arteriopathy with Subcortical Infarcts and Leukoencephalopathy (CADASIL), the most common hereditary form of stroke and dementia in the young (4), white matter infarcts lead to progressive decline in cognitive function also seen in AD and PD (4-6).

Histopathologically the decline is preceded by intra-and extracellular accumulation of Amyloid β in mostly hippocampus in AD, loss of dopaminergic cells primarily in substantia nigra in PD and in CADASIL by vascular and white matter degeneration (4-10). To diagnose these pre-symptomatic alterations (4, 5, 7-12), non-invasive methods are of particular interest to allow earlier pharmacological treatment or lifestyle adaptations, as elements towards a better quality of life for affected persons (6, 13-15). So far conventional neuroimaging methods fail to detect these alterations of early disease stages (16-18). It has been shown that biomechanical properties of brain tissue are altered by histopathological changes (19-24) and magnetic resonance elastography (MRE) as *in-vivo,* non-invasive technique, is able to measure local biomechanical/viscoelastic properties of biological tissues (19, 20).

In two of the subject studies MRE was used for measuring local viscoelastic changes in AD and PD to further assess the usability of MRE as a clinical tool to reveal mechanical shifts in hippocampus, the midbrain, substantia nigra and cortex. The shifts were correlated to the histopathology of AD and PD for diagnosis and prognosis of early disease stages. Regular physical exercise, enriched environment (ENR) as well as the involvement in daily life problem solving decelerates degenerative processes, acts neuroprotectively and increases the number of newborn cells integrating into existing circuits (25, 26). These effects were subject of the study with CADASIL mice and ENR an additional investigation area in the study of AD. CADASIL patients carry dominant mutations in the *notch3* gene, which is required for the function of small arteries and has been found to be expressed in neural precursor cells (4, 27). In CADASIL early cellular features that have an effect on neuronal plasticity still need to be further elucidated to then enable MRE as a potential early detection method (27).

In study 1 we correlated early histopathological changes in hippocampus and cortex, primarily affected brain areas in AD to alterations in viscoelasticity via MRE scans using the APP23 mouse model at three disease time points. The mice were kept in a standard (STD) and enriched environment (ENR) in order to analyze a potential environment effect on the disease progression and on MRE parameters.

In study 2 the non-transgenic 1-methyl-4-phenyl-1,2,3,6-tetrahydropyridin hydrochloride (MPTP) mouse model of PD was used to correlate MRE parameters in the substantia nigra, hippocampus

and midbrain to histopathology.
In study 3, mice overexpressing wild type Notch3 and mice overexpressing Notch3 with a CADASIL mutation were kept in RUN and ENR cages. The effects of an increase in physical activity and/or more demanding environmental conditions at early disease stages were compared in their ability to restore neurogenesis .and enhance the survival of neurons

2. Methodology

2.1 Animals

Transgenic mice were bred in the Research Institutes for Experimental Medicine of the Charité Berlin (FEM). During experiments, all animals were kept in a temperature- and humidity-controlled colony room and maintained on a light/dark cycle of 12/12h with ad libitum access to food and water. The experiments were approved by the local animal ethics committee (Landesamt für Gesundheit und Soziales, Berlin) and carried out in accordance with the European Communities Council Directive of 22 September 2010 (10/63/EU). The mice were randomly assigned to the experimental groups, the investigators blinded towards the groups.

2.1.1 APP23 mouse model of AD

Female six weeks old transgenic APP23 mice (APP23) with a C57BL/6J background expressing human APP751 cDNA with the Swedish double mutation under the murine THY-1, 2 promoter (43) were used in study 1. The genotype was confirmed by PCR following ear punches (Primers: APP ct forward: 5' GAA TTC CGA CAT GAC TCA GG 3', APP ct reverse: 5' GTT CTG CTG CTG CAT CTT CGA CA 3'. Female six weeks old C57BI/6J mice were used as controls (CTR, Charles River, Sulzfeld, Germany).

2.1.2. MPTP mouse model of PD

Female eight to ten weeks old C57BI/6N mice (Charles River, Sulzfeld, Germany) received three intraperitoneal (i.p.) injections of MPTP-HCl /dissolved in 0.9% NaCl at a dose of 20 mg/kg bodyweight every 24 h. Control animals (CTR) were injected with 0.9% NaCl. MPTP lesions dopaminergic neurons in the SN, reduces dopamine in the striatum and also in the hippocampus, which is partly innervated by dopaminergic fibers from the SN (9, 28). The dopamine depletion leads to motor symptoms comparable to those in PD patients and impairs hippocampus-dependent learning and memory functions (28).

2.1.3. TgN3^{R169C} mouse model for CADASIL

Female eight to twelve weeks old mice carrying the R169C point mutation at exon 4 of the *Notch3* gene, which is known to cause the pathological features of CADASIL (4, 29) and TgN3^{WT} mice expressing wildtype Notch3 serving as a control for the mutation were used in study 3. These two mouse strains show a 4-fold overexpression of either the mutated or the wildtype *Notch3* transcript and protein. The genotype was confirmed by PCR following tail biopsies (Primers: Notch3 forward: 5′ TTC AGT GGT GGC GGG CGTC 3′ ; Notch3 reverse: 5′GCC TAC AGG TGC CAC CAT TAC GGC3′; Vector forward: 5′AAC AGG AAG AA T CGC AAC GTT AAT3′ ; Vector reverse: 5′ AAT GCA GCG ATC AAC GCC TTC TC3′). The FVB/N background strain obtained from Janvier Labs (Le Genest-Saint-Isle, France) was used as the control (CTR) for this study.

2.2 In vivo designs

2.2.1 Study 1

Within each of the APP23 and CTR group, mice were randomly separated and placed into two different cages: STD under conventional laboratory conditions (n=5, Makrolon cages, 0.27 m x 0.15 m x 0.42 m) and larger cages (0.74 m x 0.3 m x 0.74 m, n=10) for ENR with weekly new assembled tubes, boxes and plastic houses. The mice remained in their cages for either one week, twelve or 24 weeks until MRE measurement. A MRE scan for baseline data was performed on ten mice aged six weeks of each of the CTR and APP23 group. In total twelve different groups were submitted to MRE and a baseline measurement group of each genotype. After MRE measurement mice were anaesthetized with Ketamine/Xylacine and transcardially perfused with phosphate buffered saline (PBS) and 4% paraformaldehyde (PFA). Fig.1 in (30) shows the experimental procedures.

2.2.2 Study 2

Animals were randomly divided into seven groups of n=5. All animals, except the histological counterparts for the baseline measurement, were treated i.p. with MPTP. One group (n=5) underwent MRE-imaging the day before MPTP treatment (-3 days post-injection (dpi)) as baseline and three, six, ten, 14 and 18 days after the last MPTP injection (3, 6, 10, 14, 18dpi). At each of these time points and MRE measurement times, animals of the corresponding histological group (n=5) were perfused as in study 1. Fig.1 in (31) shows the experimental procedures.

2.2.3. Study 3

131 eight to twelve weeks old female FVB/N (WT), TgN3^{R169C} (CADASIL) and TgN3^{WT} mice were separated into groups housed in three different cage conditions. Mice maintained in STD or in ENR (as in study 1, n=2-5 for STD, n=5-10 for ENR). In the third cage condition (RUN, n=2) mice were held in conventional cages and provided with a running wheel (Tecniplast, Italy). Wheel turns were

recorded by LCD counters to monitor the activity. Animals were kept in their cages for short (28 days) or long duration (six months). Before exposure to their cages, mice received three i.p. injections of the mitotic marker 5-bromo-2-deoxyuridine (BrdU) with an interval of 4 hours. It labels proliferating cells for the evaluation of the long-term survival under the influence of wild type and mutated Notch3 overexpression as well as in RUN and ENR. A separate set of FVB/N, CADASIL and TgN3^{WT} mice (corresponding to the age of the 28 days groups) under STD cage condition was tested on the Rotarod to assess motor coordination skills. Anaesthesia and perfusion were performed as in study 1. Fig.1 in (32) shows the procedures.

2.3 Magnetic resonance elastography (MRE)

MRE (study 1 and 2) was performed on a 7 tesla MRI scanner as described in (20). Mouse brains were mechanically stimulated via vibrations applied to a toothbar with an air-cooled Lorentz coil, whilst they were under inhalational anesthesia with isuflorane/oxygen. The imaging sequence was altered for MRE by sinusoidal motion sensitizing gradient (MSG) in the through-plane direction with a strength of 285 mT/m, a frequency of 900 Hz and 9 periods. Further imaging parameters were: 128x128 matrix, 25 mm FoV, 14.3 ms TE, 116.2 ms TR, 8 time steps over a vibration period. Four axial slices with a thickness of 1 mm were acquired. A 2D-Helmholtz inversion was performed, yielding the complex shear modulus G*. The real part of G*, G′=Re(G*), represents tissue elasticity mainly determined by different cell types, while the imaginary part G″=Im(G*) represents viscosity determined by density and geometry of cellular networks. The regions of interest (ROI's), hippocampus and cortex, were manually selected by outlining its anatomical structure from T2w MRI images (Fig. 1).

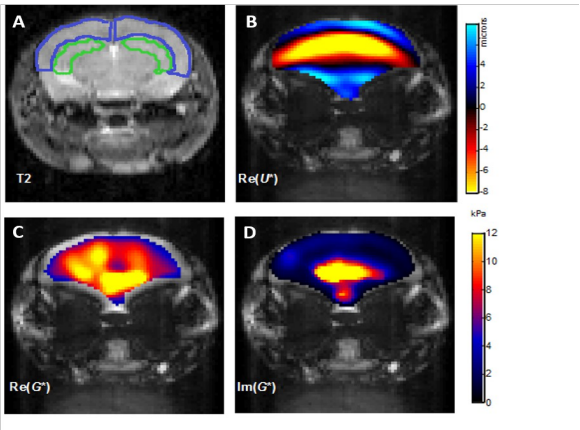

Figure 1: Representations of the MRI signal (A), shear waves (B), storage (C) and loss modulus (D) in the mouse brain overlaid with anatomic information obtained by MRI. Regions of interest: Cortex (blue line) and hippocampus (green line) were marked in T2w-MRI in (30).

2.4 Rotarod

Motor Coordination (study 3) was trained and tested on an accelerating Rotarod apparatus (TSE Systems) over three days. Day one and two were training days in four trials and animals were tested in three trials on day three with an inter-trial interval of 20 min. After 30 min habituation five mice were placed in separate sections of the apparatus on rotating rods. Acceleration happened in six

steps from four to 40 rpm with a running time of two min. The latency to drop off and acceleration phase were recorded with the TSE Software.

2.5 Histology and cell quantification

2.5.1 Immunohistochemistry

To quantify the number of cells with intracellular Aβ, newborn (proliferating) cells, microglia/macrophages and dopaminergic neurons, separate one-in-twelve (study 1) or one-in-six series (study 2 and 3) of free-floating brain sections were stained for 4G8- (Aβ; study 1), BrdU- (newborn cells; study 3), Iba1- and TH (microglia/macrophages and dopaminergic neurons; study 2) detection. Briefly, after pretreatment with H2O2 and HCl (the latter only for BrdU-detection), sections were blocked with PBS+ (0.1% Triton, 3% donkey serum) before being incubated overnight with diluted primary antibodies. The next day, sections were incubated with diluted biotinylated secondary antibodies followed by ABC reagent before visualization by 3,3'-Diaminobenzidine (DAB)-NiCl staining.

2.5.2 Immunofluorescence

For a more detailed investigation of neuronal and astrocytic cell types, a triple fluorescent staining against BrdU, the specific endogenous marker for Neuronal Nuclei (NeuN) and the specific marker S100β for mature astrocytes was performed in study 3. Therefore, a one-in-six series of free-floating brain sections of each animal was pretreated with HCl, followed by overnight incubation at 4 °C with primary antibodies against rat anti-BrdU, mouse anti-NeuN and rabbit anti-S100β. The next day, sections were incubated with fluorescent secondary antibodies RhodamineX, Alexa 647 and Alexa 488. Brain sections were mounted on object slides and coverslipped.

2.5.3 Histological stainings

For Congo-red staining (study 1) tissue sections were washed with PBS and mounted on slides. First, they were incubated for 5 min in matured haemalaun. Then they were put under running tap water for 10 min followed by exposure to solution 1a (saturated alcoholic sodium chloride solution: 2% NaCl in 80% ethanol, 1% aqueous NaOH per 100 ml) for 20 min. They were placed in solution 2a (solution 1 with alkaline Congo red) for 45min. Here, the alkaline was added just before use. They were washed, dehydrated, and mounted with cover glass for quantification manually under 200x magnification of the light microscope as above in hippocampus and cortex.
To determine the total cell number in the cortex and hippocampus (study 1), SN, midbrain and hippocampus (study 2) sections were stained with the fluorochrome 4′6-diamidino-2-phenylindole (DAPI), which binds to the DNA thereby labeling cell nuclei. Free-floating one in twelve-section series were rinsed and incubated with PBS-diluted DAPI for 7 min, washed again and afterwards mounted on microscope slides and coverslipped.

2.5.4 Cell quantification

A Leica DMRE microscope equipped with StereoInvestigator (MicroBrightfield) software was used to quantify 4G8-positive (Aβ+, study 1). Aß was counted in the cortex and hippocampus in the right and the left hemisphere in five APP23 mice of each age group. There was no 4G8-immunoreactivity in the CTR. The brain areas were traced with a 5x objective in areas based on the mouse brain atlas between Bregma -0.58 and -4.49 mm. Plaques were counted on every twelfth section with a 100x objective in oil. The software randomly arranged counting frames of 60 µm x 60 µm × 60 µm with a sampling grid of 500 µm × 500 µm over the ROI and an Optical Dissector height of 20 µm starting 5 µm below the top surface. The total number of cells per selected brain region was automatically calculated based on the settings described before from manually counted cell numbers in the counting frames. This microscope was also used to quantify DAPI-positive (DAPI+) cells. In study 1 DAPI+ cell nuclei in the hippocampus of five mice and three mice for cortex per group of both genotypes were counted including every sixth section applying the same parameters as when counting Aβ+ cells. The DAPI+ cells in midbrain, SN and hippocampus in study 2 of two mice per group were analyzed. Two sections in an interval of twelve were counted using a sampling grid size of 250x200 µm in the the SN, 600x600µm in the midbrain and hippocampus. In study 2 Iba1-positive cells (Iba1+) were quantified with the same Leica DMRE microscope and the StereoInvestigator software in four sections with an interval of six using a sampling grid of 150x120 µm. In all brain sections in study 2 a counting frame of 60x60 µm without guard dissector height was used.

Extracellular plaques, visualized with Congo red, were counted manually in all APP23 mice with 200x magnification of a light microscope (Zeiss Axioskop, Germany) in the same areas as described above in study 1.Four stained brain slices of each mouse were analyzed for TH positive cells (TH+; study 2) in the SN, including pars compacta and pars reticulata. Cells were manually counted via 40x magnification of the same light microscope and multiplied by six to obtain an estimated absolute number of cells per SN. BrdU/DAB-positive (BrdU+, study 3) cells were counted in the dentate gyrus (DG) including the subgranular zone (SGZ) of nine sections per animal under 200x magnification using the same light microscope as above.

To detect co-labeled BrdU/NeuN-positive (BrdU+/NeuN+) and BrdU/S100β-positive (BrdU+/S100β+) cells in study 3, 50 BrdU+ cells across the rostrocaudal extent of the DG were sequentially scanned (z-stacks) using a confocal microscope (Leica TCS SP2). The obtained ratio was used to determine the absolute cell number. The confocal images were taken using the 40x immersion oil objective of the Leica DM 2500 confocal microscope. To get a whole image of the examined cells, 19 sequentially taken images were z-stacked. The distance between the images was 0.34 µm. Fiji for Windows 32 was used to adjust brightness and contrast.

2.6 Statistical analysis

Graphical and statistical analyses were accomplished using GraphPad Prism 5.0. The level of statistical significance was set at $p \leq 0.05$. IBM SPSS statistics 19 was used in study 1 and 2, data in study 3 were statistically analyzed using IBM SPSS Statistics 23.

In study 1 a three-way ANOVA was applied with factors genotype (g, CTR vs. APP23), cage condition (c, STD vs. ENR) and duration of the specific cage condition (d, one week vs. twelve weeks vs. 24 weeks). To analyze the histological data of the 4G8 staining in the APP23 mouse group, a two-way ANOVA with factors c and d was performed. There were only very sparse extracellular plaques stained with Congo Red in a few APP23 mice aged 24 weeks, here no statistical analysis was performed.

In study 2 the homogeneity of variance was tested by Levene test. One-way ANOVA was performed for the data from the quantification of TH+ and Iba1+ cells and one-way repeated measures (RM) ANOVA for MRE data. The data from the DAPI counts were not statistically evaluated, because only n=2 per time point were quantified.

In study 3 a two-way ANOVA was applied to analyze the effects of the factors Genotype (g), Cage Condition (c) and their interaction (cg) on the numbers of BrdU+, BrdU+/NeuN+ and BrdU+/S100β+ cells. Running wheel activity during the short-term (28 days), long-term (6 months) and Rotarod performance were analyzed by a one-way ANOVA. In case of interaction of the factors, pairwise comparisons were done using the Bonferroni post-hoc test in all studies.

Table 1: List of all substances used in the experiments and analysis with dilution and dosage

Substance	Abbreviation	Dilution	Company
1-Methyl-4-phenyl-1,2,3,6-tetrahydropyridine Hydrochloride	MPTP-HCl	10 mg/ml, 20 mg/kg BW	Sigma-Aldrich
5'-Bromo-2'-deoxyuridine	BrdU	10 mg/ml, 50 mg/kg BW	Sigma-Aldrich
Rhodamine X rat		1:250	Dianova
Alexa 488 rabbit		1:1000	Invitrogen
Alexa 647 mouse		1:300	Dianova
Nickelchloride	Ni2Cl	0.4 mg/ml	Sigma-Aldrich
Ionized calcium-binding adaptor molecule 1 antibody rabbit	anti-Iba1 rb	1:1000	Wako
Vectastain® ABC Elite kit	ABC reagent	9 l¼l/ml	Vector Laboratories
3,3'-Diaminobenzidine	DAB	0.025 mg/ml	2-methylbutane
4G8 mouse-antibody	4G8	1:1000	BioLegend
Congo red		6mg/ml	Sigma-Aldrich

Hydrochloric acid	HCl	2 M	Merck
Ketamine hydrochloride 10%	Ketamine	0.75 ml/25 g BW	WDT
Paraformaldehyde	PFA	40 g/l	Sigma-Aldrich
Phosphate-buffered saline	PBS		Roth
Triton X-100 10%	Triton	10ml/l	Fluka
Hydrogen peroxide 30%	H2O2	20 ml/l	Roth
2-methylbutane	C15H12	undiluted	Sigma-Aldrich
Xylacine (Rompun) 2%	Xylacine	0.25 ml/25 g BW	Provet AG
4′6-diamidino-2-phenylindole	DAPI	1:1000	Thermo Scientific
Astrocytes anti-S100β rabbit	anti-S100β	1:150	Abcam
Neuronal nuclei antibody mouse	Anti-NeuN ms	1:1000	Milipore
5'-Bromo-2'-deoxyuridine antibody rat	anti-BrdU	1:500	AbD serotec
Biotin rat		1:125	Dianova
Tyrosinhydroxylase antibody mouse	TH	1:10000	Sigma-Aldrich

3. Results

3.1 Study 1: MRE is sensitive to detect alterations in viscoelasticity occurring on a cellular scale associated with early histopathological changes in a mouse model of AD.

MRE of hippocampus shows viscosity of CTR mice is higher than in the APP23: This becomes more obvious over time ($F(2,78)=7.222$, $p=0.001$, adult APP23 vs. adult CTR $p<0.001$) as hippocampal viscosity is increasing only in the CTR group ($F(2,78)=7.222$, $p=0.001$).
Viscosity in the hippocampus of the CTR group also increases after exposure to ENR ($F(1,80)=4.798$, $p=0.032$, STD vs. ENR: $p=0.007$). ENR restored the lower cell numbers in APP23 mice leading to similar cell levels in APP23 and CTR mice, but only transiently ($F(2,54)=2.822$, $p=0.069$, one week: $p=0.002$). The correlation of viscosity with DAPI+ cells was significant in APP23 mice under ENR cage conditions ($p=0.01$) indicating enhanced viscosity here relates to higher cell numbers in the adolescent mice.
DAPI+ cell numbers in the hippocampus are generally lower in APP23 compared to CTR mice under STD cage condition, though cell numbers also decrease with aging in CTR ($F(2,58)=21.688$, $p\leq0.001$, one vs. twelve vs. 24 weeks, $p \leq 0.001$). Disease progression in APP23 corresponds to decreased cell numbers even more in adolescent ($p=0.001$) and adult ($p \leq0.0001$) mice ($F(2,55)=4.575$, $p<0.015$).
Hippocampal elasticity of adolescent APP23 is lower compared to same aged CTR ($p=0.018$) but

increases with age ($F(2,78)=3.928$, $p=0.024$). Correlation of hippocampal elasticity to Aβ+ cells in the hippocampus shows that in ENR an increased amount of cells carrying Aβ may be the reason for enhanced elasticity. In general Aβ+ cells show a decreasing trend ($F(2,28)=3.199$, $p=0.059$) from young-adult to adult mice ($p=0.057$).
In cortex, elasticity and also Aβ+ cells increase with age ($F(2,82)=3.242$, $p=0.045$; $F(2,30)=3.660$, $p=0.041$). DAPI+ cells in cortex decrease with age ($F(2,33)=8.017$, $p=0.002$).

3.2. Study 2: Viscoelasticity changes in the midbrain, hippocampus and SN due to the MPTP-induced dopaminergic neurodegeneration.

MRE parameters at -3dpi revealed a basic difference in viscosity between the various brain areas in baseline measurements ($F(2,14)=5.396$, $p\leq0.05$). There is a higher viscosity in the midbrain (1.836 ±0.043 kPa) than in the hippocampus (1.426 ±0.051 kPa, $p\leq0.05$).
In the SN a decrease in both elasticity and more so viscosity were seen following MPTP treatment with some restoration over time: Elasticity G'($F(5,29)=4.274$, $p\leq0.01$,) and viscosity G"($F(5,29)=8.350$, $p\leq0.001$). This decrease in elasticity and viscosity in SN post MPTP treatment correlates to MPTP induced neurodegeneration in the SN: TH+ dopaminergic neurons were lower at all time points ($F(5,28)=7.499$). The immediate reduction of TH+ dopaminergic neurons following treatment was 57%, persisting until the last time point. MPTP also reduces the cell amount (DAPI+ cells) in the SN with a slight restoration over time (224700 (±6967) cells at -3dpi to 164083 (±8417) cells at 6dpi. The Iba1+ cell count revealed that MPTP induces a transient increase of microglia and macrophages in the SN as a sign for a local inflammatory reaction ($F(5,28)=5.706$, $p\leq0.01$, $p\leq0.05$). Directly after MPTP treatment (3dpi) Iba+ cells were significantly more numerous (-3dpi vs. 3dpi: $p\leq0.05$), although ceasing until baseline levels at 18dpi. The initially elevated amount of Iba+ cells in the SN is not reflected in MRE.
In the midbrain an increase in both elasticity and viscosity were seen post MPTP treatment: G'($F(5,29)=6.702$, $p\leq0.001$) and G"($F(5,29)=6.895$, $p\leq0.001$). MPTP reduces the amount of DAPI+ cells in the midbrain with a total cell amount from 1834800 (±116400) to 1333800 (±60600) cells at -6dpi. In contrast to the SN, the midbrain had increased tissue stiffness in response to MPTP, the lower total amount of DAPI+ cells does not correlate with this finding.
In hippocampus MPTP also induces a transient increase of viscosity and elasticity, G'($F(5,29)=11.75$, $p\leq0.001$) and G"($F(5,29)=8.075$, $p\leq0.001$) indicating a transient tissue stiffening six days after treatment cessation. A total amount of 1385400 (±155400) DAPI+ cells at -3dpi and a transient rise at 6dpi up to 1468200 (±89400) cells were seen in hippocampus. The increased viscosity and elasticity in the hippocampus correlates to a higher DAPI+ cell count.

3.3 Study 3: Hippocampal neurogenesis could not be stimulated by RUN or ENR, indicating a disturbed neurogenic process in mice overexpressing Notch3 and with a CADASIL

mutation.

In the long-term STD group, notably but insignificant, WT and CADASIL mice displayed more BrdU+ and BrdU+/NeuN+ cells than $TgN3^{WT}$ ($F(4,53)=2.415$ $p=0.06$) indicating reduced survival of newborn cells in $TgN3^{WT}$ mice.

Only in the WT short-term group RUN and ENR increased survival of BrdU+/S100β+ and of BrdU+/NeuN+ cells, $F(4,60)=4.495$, $p < 0.01$). During 28 days $TgN3^{WT}$ have more running wheel activity in 24h than the other two mouse types ($F(2,543)=84.66$, $p<0.001$). Considering the most relevant first five days for neurogenesis, WT and $TgN3^{WT}$ ran similar distances whereas CADASIL mice ran significantly less in 24h ($F(2,92)=22.34$, $p < 0.001$).

During six months; running wheel activity was strongly reduced in both $TgN3^{WT}$ and CADASIL mice compared to WT ($F(2,1569)=229.7$, $p < 0.001$) with CADASIL mice running even less than $TgN3^{WT}$. The running distance per month of the CADASIL mice decreased further over time ($F(5,8)=8.121$, $p < 0.01$). In the long-term group in CADASIL mice more newly generated BrdU+ cells differentiate into astrocytic S100β+ cells than in WT mice ($F(2,59)=4.030$,$p<0.05$) resulting in an age-dependent astrogliosis.

Rotarod performance revealed $TgN3^{WT}$ and CADASIL mice spent less time on the rod than WT mice ($F(2,16)=6.309$, $p < 0.01$), indicating a motor deficit in both transgenic mouse lines.

4. Discussion

4.1. MRE detects early histopathological alterations as viscoelastic changes in hippocampus of an APP23 mouse model of AD

Viscosity, which depends on structural and functional integrity of cellular networks (21-24, 33), increases with age in the CTR within the time frame studied here. Neuronal disintegration due to aging may be the reason for a disturbed cellular structure and absorb strain energy (33, 34) resulting in increased viscosity. Viscosity in the hippocampus of APP23 mice is in general lower than in the CTR and a rise in viscosity parameters does not occur in APP23 mice. This correlates to a significant neuronal loss reflected in a progressively lower DAPI+ cell count in the APP23 compared to the CTR and also disease progression is known to result in decreased neuronal functionality (8, 35-38).

Elasticity, an indicator for cell density, is lower in the hippocampus of adolescent APP23 mice than in the age-matched CTR. This points towards very early pathological changes on a cellular level as intracellular Aβ can already be detected (8, 38). The rise in elasticity parameters observed with disease progression in APP23 mice may be linked to the slight but non-significant increase of Aβ+ cells and the externalization of Aβ with time, also affecting the mechanical integrity by filling the interstitial space. Intracellular amyloid β has also been shown to induce neuronal cell death (37). We speculate that neurons undergoing apoptosis exhibit different biomechanical characteristics as they go through considerably different morphological stages than healthy cells (39).

ENR transiently increased the total number of cells in the hippocampus of APP23 mice, keeping it on a higher level than mice in STD. This may be due to neuroprotective effects of ENR and/or due to enhanced neurogenesis (25, 39, 40), although a reduction of DAPI+ cells over time with disease progression can also be observed in ENR. The cell loss might be too severe for ENR to counteract and a restorative effect is also not seen in the viscous or elastic properties of the hippocampus. In CTR mice, ENR increases hippocampal viscosity, although cell numbers in CTR are not changed. Hence the component altered by ENR might not be just cellular, but growth of axons and synapses induced by ENR compacting the network (25, 40, 41).

In summary, elastic and viscous properties of hippocampal tissue are lower in APP23 mice at early disease stages compared to age-matched CTR mice. Only for viscosity, this difference becomes more pronounced with disease progression. ENR fails to stop the progressive neuronal loss and the decrease of viscosity in the long-term, indicating that it is therapeutically not suitable to prevent or halt the changes in tissue mechanical properties in AD. MRE has overall shown to be sensitive to detect specific alterations in viscosity and elasticity associated with early histopathological changes in AD and in aging processes.

4.2 MRE is sensitive to detect local decreased viscoelasticity in the SN correlating to reduced neurons due to MPTP-induced neurodegeneration

MPTP decreases viscosity (cellular network) and - to a lesser extent - elasticity (cell density) in the SN six days after treatment cessation. The SN is densely packed with dopaminergic cell bodies and their extensions (42). MPTP reduces TH+ dopaminergic neurons already three days after treatment, though MRE parameters are unchanged until 6dpi. TH activity has been shown to decrease first, followed by an obvious reduction of neurons after MPTP treatment (42). Here the number of DAPI+ cells correlates with the late changes in viscosity, hence the changed viscosity and partly elasticity reflects the dopaminergic neurodegeneration in the SN.

In the hippocampus a transient rise of elasticity and viscosity correlates to the total amount of cells being elevated at 6dpi. The findings of Klein et al. underline this observation by showing an increased stiffness in hippocampus following MPTP treatment (14). Besides dopamine depletion, MPTP provokes an inflammatory response. It initially leads to a higher amount of microglia and macrophages in the SN and hippocampus, which diminishes after treatment cessation (43). In our study, the initially increased amount of Iba+ cells in the SN is not reflected in MRE parameters. MRE may not be suitable for detecting microglia or macrophages as small, transient, local inflammation at least in particular structures like the SN and hippocampus (43). In a study by Millward et al. (43) MRE did not respond to mild inflammation in a C57Bl/6 mouse model of autoimmune encephalomyelitis. Only in mice with a more severe reaction MRE showed altered brain elasticity during the course of the disease correlated to macrophages and microglia.

MRE parameters of the midbrain were higher after treatment in response to MPTP. The lower amount of DAPI+ cells does not correlate with this, but MPTP is not known to lead to dopaminergic neurodegeneration in the midbrain (9, 10). The discrepancy between midbrain MRE and histology may be due to the midbrain being larger than the SN with several white matter tracts, which have been shown to be stiffer than grey matter in humans (44-46). In correlation to this, a higher basic viscosity was also seen in the midbrain compared to the hippocampus in healthy mice at -3dpi.

To summarize, we demonstrated that changes in the amount of dopaminergic neurons in the SN of MPTP-lesioned mice are detectable by MRE. The initially elevated amount of inflammatory cells in the SN however is not reflected in MRE parameters. This study contributes to the investigation of the missing link between histopathological alterations and biomechanical constants in small brain areas affected in PD and a decrease of viscoelastic properties of the adult brain is probably based on the reduced number of neuronal cells.

4.3 RUN or ENR failed to induce neurogenesis in both transgenic mouse lines probably due to Notch3-dependent micromilieu changes as a vascular-independent mechanism.

As neurogenesis in the $TgN3^{WT}$ mice is decreased only in the long-term STD group, there has to be a counteracting mechanism in younger mice which is lost during aging. The decreased neurogenesis in $TgN3^{WT}$ mice of the long-term group replicates the finding of our previous study in six-months-old $TgN3^{WT}$ mice. Lower neurogenesis levels were found four weeks after BrdU cell labeling (47) and were still evident five months later in $TgN3^{WT}$, thus Notch3 overexpression seems to suppress cell proliferation. Despite a reduced motor coordination, $TgN3^{WT}$ ran more in the running wheel than WT mice in the short-term group. RUN or ENR are normally potent neurogenic stimulants (25, 26, 41) and in WT mice, as expected, they increased hippocampal neurogenesis (25, 26, 41). Both RUN and ENR failed to stimulate neurogenesis in $TgN3^{WT}$ mice however, although under short-term STD conditions basal neurogenesis is not decreased. In our previous work, we demonstrated that the proliferative activity of neural precursor cells was potentially reduced by Notch3 overexpression (47), which might in turn prevent their activation via ENR or RUN (48). The $TgN3^{WT}$ long-term group showed reduced physical activity and RUN or ENR failed to stimulate neurogenesis. As they ran more than the WT in the short-term group with no effect on neurogenesis levels, physical activity may not work as a supportive therapy unless Notch3 is regulated too. In ENR, social interaction with more mice and changing interior designs are extra stimulants, hence other functions than solely physical fitness could be affected by mutated Notch3. RUN or ENR did also not increase neurogenesis in CADASIL mice. They showed reduced physical activity in the running wheels in both durations and impaired motor coordination on the Rotarod. Overexpression of mutated Notch3 may disturb the milieu of precursor cells preventing them from reacting to RUN or ENR (47, 48). Functional Notch3 and also its available amount in precursor

cells are probably essential for the regulation of hippocampal neurogenesis. In the CADASIL long-term group neurogenesis is not decreased, though more new cells differentiated into astrocytes. Astrocytes have been shown to support the proliferation and differentiation of stem cells in vitro (49). A higher amount of astrocytes could be a counteracting mechanism for a disturbed neurogenesis due to mutated Notch3, although it could still not be stimulated by RUN or ENR. We also found a higher amount of astrocytes in WT animals induced by short-term RUN, replicated by previous findings showing different stimuli affect different subpopulations of hippocampal cells: RUN here also stimulated the formation of astrocytic cells (49-51).
Conclusively adult hippocampal basal neurogenesis itself is not altered in mice of the short-term group in both transgenic mouse lines. Neurogenesis however could not be stimulated by RUN or ENR of either duration, indicating a disturbance not reflected on the basal neurogenesis level. Maybe there is an independent regulatory role of Notch3 in neurogenesis, as all of this happens while there are no deficits in microcirculation or the vascular network (50, 52). Cell intrinsic deficits in Notch3 signaling might change the micromilieu and could be a vascular-independent mechanism regulating neurogenesis in CADASIL patients, supporting the development of cognitive deficits (50, 52).

5. Conclusion

An aging society combined with physical inactivity increases prevalence of neurodegenerative diseases (1-3). Early detection of these diseases to start an early therapy and maintaining physical fitness can possibly, but not solely counteract and postpone their outbreak. The present results clearly show that (1) potential detection of AD at a still histologically early stage prior to clinical symptoms might be possible with MRE, which has also shown to be sensitive to histopathological changes in smaller brain areas as effected in PD. MRE could possibly be further used to detect early histopathological changes in other genetic neuropathological diseases like CADASIL. (2) Changes in the micromilieu due to the influence of Notch3 overexpression or accumulation of Aβ in AD impact adult hippocampal neurogenesis, neurodegeneration and cell survival visibly at early disease stages. .Physical exercise and ENR as known enhancers of neurogenesis and acting neuroprotective might not be enough as a supportive therapy.

6. Bibliography

1. Guure CB, Ibrahim NA, Adam MB, Said SM. Impact of Physical Activity on Cognitive Decline, Dementia, and Its Subtypes: Meta-Analysis of Prospective Studies. Biomed Res Int. 2017;9016924.
2. Barnes DE, Yaffe K. The projected effect of risk factor reduction on Alzheimer's disease prevalence. The Lancet Neurology 2011;10:819–828.

3. Murray DK, Sacheli MA, Eng JJ, Stoessl AJ. The effects of exercise on cognition in Parkinsons's disease: A systemic review. Translational Neurodegeneration 2014;3:5.
4. Joutel A, Corpechot C, Ducros A, Vahedi K, Chabriat H, Mouton P, Alamowitch S, Domenga V, Cécillion M, Marechal E, Maciazek J, Vayssiere C, Cruaud C, Cabanis EA, Ruchoux MM, Weissenbach J, Bach JF, Bousser MG, Tournier-Lasserve E. Notch3 mutations in CADASIL, a hereditary adult-onset condition causing stroke and dementia. Nature 1996;383:707-710.
5. Nelson PT, Alafuzoff I, Bigio EH, Bouras C, Braak H, Cairns NJ, Castellani RJ, Crain BJ, Davies P, Del Tredici K, Duyckaerts C, Frosch MP, Haroutunian V, Hof PR, Hulette CM, Hyman BT, Iwatsubo T, Jellinger KA, Jicha GA, Kövari E, Kukull WA, Leverenz JB, Love S, Mackenzie IR, Mann DM, Masliah E, McKee AC, Montine TJ, Morris JC, Schneider JA, Sonnen JA, Thal DR, Trojanowsi JQ, Troncoso JC, Wisniewski T, Woltjer RL, Beach TG. Correlation of Alzheimer disease neuropathologic changes with cognitive status: a review of the literature. J Neuropathol Exp Neurol 2012;71:362–381.
6. Pillon B, Dubois B, Bonnet AM, Esteguy M, Guimaraes J, Vigouret JM, Lhermitte F, Agid Y. Cognitive slowing in Parkinson's disease fails to respond to levodopa treatment: the 15-objects test. Neurology 1989;39:762-768.
7. Bondareff W. Age-related changes in brain extracellular space affect processing of amyloid-beta peptides in Alzheimer's disease. J Alzheimers Dis. 2013;35:1-6
8. Selkoe DJ. Alzheimer's disease: genes, proteins, and therapy. Physiological reviews. 2001;81:741-766.
9. Gasbarri A, Sulli A, Packard MG. The dopaminergic mesencephalic projections to the hippocampal formation in the rat. Prog Neuro-Psychopharmacol& Biol Psychiat 1997;21:1–22.
10. Jackson-Lewis V, Jakowec M, Burke RE, Przedborski S. Time course and morphology of dopaminergic neuronal death caused by the neurotoxin 1-methyl-4-phenyl-1,2,3,6-tetrahydropyridine. Neurodegeneration 1995;4: 257–269
11. Hirsch E, Graybiel AM, Agid YA. Melanized dopaminergic neurons are differentially susceptible to degeneration in Parkinson's disease. Nature 1988;334: 345–348.
12. Joutel A, Monet-Lepretre M, Gosele C, Baron-Menguy C, Hammes A, Schmidt S, Lemaire-Carrette B, Domenga V, Schedl A, Lacombe P, Hubner N. Cerebrovascular dysfunction and microcirculation rarefaction precede white matter lesions in a mouse genetic model of cerebral ischemic small vessel disease. J Clin Invest 2010;120: 433-445.
13. Roberson ED, Mucke L. 100 years and counting: prospects for defeating Alzheimer's disease. Science 2006;314:781–784.
14. Klein C, Rasinska J, Empl L, Sparenberg M, Poshtiban A, Hain EG, Iggena D, Rivalan M, Winter Y, Steiner B. Physical exercise counteracts MPTP-induced changes in neural precursor

cell proliferation in the hippocampus and restores spatial learning but not memory performance in the water maze. Behav Brain res. 2016;307: 227–238.
15. Schreiber S, Vogel J, Schwimmer HD, Marks SM, Schreiber F, Jagust, W. Impact of lifestyle dimensions on brain pathology and cognition.Neurobiol Aging 2016;40:164–172.
16. Al-Radaideh AM, Rababah EM. The role of magnetic resonance imaging in the diagnosis of Parkinson's disease: a review. Clinical imaging 2016;40:987-996.
17. Health Quality Ontario. The appropriate use of neuroimaging in the diagnostic work-up of dementia: an evidence-based analysis. Ont Health Technol Assess Ser 2014;14:1–64.
18. Schroder J, Pantel J. Neuroimaging of hippocampal atrophy in early recognition of Alzheimer's disease--a critical appraisal after two decades of research. Psychiatry research 2016;247:71-78.
19. Posnansky O, Guo J, Hirsch S, Papazoglou S, Braun J, Sack I. Fractal network dimension and viscoelastic powerlaw behavior: I. A modeling approach based on a coarse-graining procedure combined with shear oscillatory rheometry. Physics in medicine and biology 2012;57:4023-4040.
20. Muthupillai R, Lomas DJ, Rossman PJ, Greenleaf JF, Manduca A, Ehman RL. Magnetic resonance elastography by direct visualization of propagating acoustic strain waves. Science 1995;269:1854–1857.
21. Klein C, Hain EG, Braun J, Riek K, Mueller S, Steiner B, Sack I. Enhanced adult neurogenesis increases brain stiffness: in vivo magnetic resonance elastography in a mouse model of dopamine depletion. PloS one 2014;9:e92582.
22. Freimann FB, Muller S, Streitberger KJ, Guo J, Rot S, Ghori A, Vajkoczy P, Reiter R, Sack I, Braun J. MR elastography in a murine stroke model reveals correlation of macroscopic visco-elastic properties of the brain with neuronal density. NMR in biomedicine 2013;26:1534-1539.
23. Schregel K, Wuerfel neé Tysiak E, Gemeinhardt I, Prozorovski T, Aktas O, Merz H, Petersen D, Wuerfel J, Sinkus R. Demyelination reduces brain parenchymal stiffness quantified in vivo by magnetic resonance elastography. Proc Natl Aca Sci U S A 2012;109:6650–6655.
24. Riek K, Millward JM, Hamann I, Mueller S, Pfueller CF, Paul F, Braun J, Infante-Duarte C, Sack I. Magnetic resonance elastography reveals altered brain viscoelasticity in experimental autoimmune encephalomyelitis. NeuroImage: Clinical 2012;1:81–90.
25. Kempermann G, Gast D, Gage FH. Neuroplasticity in old age: sustained fivefold induction of hippocampal neurogenesis by long-term environmental enrichment. Ann. Neurol. 2002;52:135–143.
26. Kronenberg G, Bick-Sander A, Bunk E, Wolf C, Ehninger D, Kempermann G. Physical exercise prevents age-related decline in precursor cell activity in the mouse dentate gyrus. Neurobiol. Aging 2006,27:1505–1513.
27. Irvin DK., Zurcher SD, Nguyen T, Weinmaster G., Kornblum H. I. Expression patterns of

Notch1, Notch2, and Notch3 suggest multiple functional roles for the Notch-DSL signaling system during brain development. J. Comp. Neurol. 2001; 436:167–181.

28. Marsden CD, Jenner PG. The significane of 1-methyl-4-phenyl-1,2,3,6-tetrahydropyridine. Ciba Found Symp 1987;126:239-256.
29. Joutel A, Andreux F, Gaulis S, Domenga V, Cecillon M, Battail N, Piga N, Chapon F, Godfrain C, Tournier-Lasserve E. The ectodomain of the NOTCH3 receptor accumulates within the cerebrovasculature of CADASIL patients. J Clin Invest 2000;105:597-605.
30. Munder T, Pfeffer A, Schreyer S, Guo J, Braun J, Sack I, Steiner B, Klein C. MR elastography detection of early viscoelastic response of the murine hippocampus to amyloid β accumulation and neuronal cell loss due to Alzheimer's disease. JMRI 2017;25741.
31. Hain EG, Klein C, Munder T, Braun J, Riek K, Mueller S, Sack I, Steiner B. Dopaminergic neurodegeneration in the mouse is associated with decrease of viscoelasticity of substantia nigra tissue. PLoS One 2016; 11:e0161179.
32. Klein C, Schreyer S, Kohrs F, Elhamoury P, Pfeffer A, Munder T, Steiner B. Stimulation of adult hippocampal neurogenesis by physical exercise and enriched environment is disturbed in a CADASIL mouse model. Scie Rep 2017;45372.
33. Lu Y-B, Iandiev I, Hollborn M, Körber N, Ulbricht E, Hirrlinger PG, Körber N, Ulbricht E, Hirrlinger PG, Pannicke T, Wei EQ, Bringmann A, Wolburg H, Wilhelmsson U, Pekny M, Wiedemann P, Reichenbach A, Käs JA.. Reactive glial cells: increased stiffness correlates with increased intermediate filament expression. FASEB J. 2011;25: 624–631.
34. Nieto-Sampedro M, Nieto-Díaz M. Neural plasticity: changes with age. J Neural Transm 2005;112: 3 -27.
35. Jang SS, Chung HJ. Emerging Link between Alzheimer's disease and Homeostatic Synaptic Plasticity. Neural Plast 2016;7969272.
36. Kienlen-Campard P. Intracellular Amyloid-beta 1-42, but Not Extracellular Soluble Amyloid-beta Peptides, Induces Neuronal Apoptosis. J Biol Chem 2002;277:15666–15670.
37. Sturchler-Pierrat C, Staufenbiel M. Pathogenic mechanisms of Alzheimer's disease analyzed in the APP23 transgenic mouse model. Ann N Y Acad Sci 2000;920:134–139.
38. Häcker G.The morphology of apoptosis. Cell Tissue Res. 2000; 301:5-17.
39. Beauquis J, Pavía P, Pomilio C, Vinuesa A, Podlutskaya N, Galvan V, Saravia F. Environmental enrichment prevents astroglial pathological changes in the hippocampus of APP transgenic mice, model of Alzheimer's disease. Exp Neurol 2013;239:28–37.
40. Hu Y-S, Xu P, Pigino G, Brady ST, Larson J, Lazarov O. Complex environment experience rescues impaired neurogenesis, enhances synaptic plasticity, and attenuates neuropathology in familial Alzheimer's disease-linked APPswe/PS1DeltaE9 mice. FASEB J 2010;24:1667–1681.
41. Kempermann G, Jessberger S, Steiner B, Kronenberg G. Milestones of neuronal development

in the adult hippocampus. Trends Neurosci 2004;27:447-452. 8.
42. Jackson-Lewis V, Jakowec M, Burke RE, Przedborski S.Time course and morphology of dopaminergic neuronal death caused by the neurotoxin 1-methyl-4-phenyl-1,2,3,6-tetrahydropyridine. Neurodegeneration. 1995;4:257–269.
43. Annese V, Herrero MT, Di Pentima M, Gomez A, Lombardi L, Ros CM, De Pablos V, Fernandez-Villalba E, De Stefano ME. Metalloproteinase-9 contributes to inflammatory glia activation and nigro-striatal pathway degeneration in both mouse and monkey models of 1-methyl-4-phenyl-1,2,3,6-tetrahydropyridine (MPTP)-induced Parkinsonism. Brain Struct Funct. 2015;220: 703–727.
44. Millward JM, Guo J, Berndt D, Braun J, Sack I, Infante-Duarte C. Tissue structure and inflammatory processes shape viscoelastic properties of the mouse brain. NMR Biomed. 2015;28:831-9
45. Kruse SA, Rose GH, Glaser KJ, Manduca A, Felmlee JP, Jack CR Jr, Ehman RL. Magnetic resonance elastography of the brain. NeuroImage. 2008;39:231–237.
46. McCracken PJ, Manduca A, Felmlee J, Ehman RL. Mechanical transient-based magnetic resonance elastography. Magn Reson Med. 2005;53:628–639.
47. Ehret F, Vogler S, Pojar S, Elliott DA, Bradke F3, Steiner B, Kempermann G. Mouse model of CADASIL reveals novel insights into NOTCH3function in adult hippocampal neurogenesis. Neurobiol. Dis. 2015;75:131–141.
48. Breunig J, Silbereis J, Vaccarino F M, Sestan N & Rakic P. Notch regulates cell fate and dendrite morphology of newborn neurons in the postnatal dentate gyrus. Proc. Natl. Acad. Sci. USA 2007;104:20558–20563.
49. Steiner B, Kronenberg G, Jessberger S, Brandt MD, Reuter K, Kempermann K. Differential regulation of gliogenesis in the context of adult hippocampal neurogenesis in mice. Glia 2004;46:41–52.
50. Stump G, Durrer A, Klein AL, Lütolf S, Suter U, Taylor V. Notch1 and its ligands Delta-like and Jagged are expressed and active in distinct cell populations in the postnatal mouse brain. Mech. Dev. 2002; 14:153–159
51. Seki, T. Microenvironmental elements supporting adult hippocampal neurogenesis. Anat. Sci. Int. 2003;78:69–78

Affidavit

I, Tonia Munder, certify under penalty of perjury by my own signature that I have submitted the thesis on the topic „Investigation of early histopathological changes in rodent models of Alzheimer's Disease, Parkinson's Disease and CADASIL: Brain magnet resonance elastography for early disease detection and staging correlated to histopathology and analysis of neurogenesis and cell survival" I wrote this thesis independently and without assistance from third parties, I used no other aids than the listed sources and resources.

All points based literally or in spirit on publications or presentations of other authors are, as such, in proper citations (see "uniform requirements for manuscripts (URM)" the ICMJE www.icmje.org) indicated. The sections on methodology (in particular practical work, laboratory requirements, statistical processing) and results (in particular images, graphics and tables) correspond to the URM (s.o) and are answered by me. My contributions in the selected publications for this dissertation correspond to those that are specified in the following joint declaration with the responsible person and supervisor. All publications resulting from this thesis and which I am author of correspond to the URM (see above) and I am solely responsible.

The importance of this affidavit and the criminal consequences of a false affidavit (section 156,161 of the Criminal Code) are known to me and I understand the rights and responsibilities stated therein.

_____ _____

Date Signature

Declaration of any eventual publications

Tonia Munder had the following share in the following publications:

Publication 1:
Munder T, Pfeffer ., Schreyer S, Guo J, Braun J, Sack I, Steiner B, Klein C, MR elastography detection of early viscoelastic response of the murine hippocampus to amyloid β accumulation and neuronal cell loss due to Alzheimer's disease. *JMRI*, 2017.
IF: 3.25 (2015/2016)
Contribution in detail: 80%. Performed experiments including animal handling, injections, MRE measurements, brain tissue processing, and histological staining and counting, analyzed the data, wrote the manuscript.

Publication 2:
Hain EG, Klein C, **Munder T**, Braun J, Riek K, Mueller S, Steiner B. Dopaminergic Neurodegeneration in the Mouse Is Associated with Decrease of Viscoelasticity of Substantia Nigra Tissue. *PLoS ONE*, 2016.
IF: 3.057 (2015/2016)
Contribution in detail: 10%. Partly performed histological staining and counting, data analysis and revision of manuscript.

Publication 3:
Klein C, Schreyer S, Kohrs FE, Elhamoury P,. Pfeffer A, **Munder T**, Steiner B.
Stimulation of adult hippocampal neurogenesis by physical exercise and enriched environment is disturbed in a CADASIL mouse model. *Sci. Rep,* 2017.
IF: 5.228 (2015/2016)
Contribution in detail: 10%. Partly performed experiments including animal handling, injections, and behavioral experiments, histological staining and revised the manuscript.

Signature, date and stamp of the supervising university teacher

_____

Signature of the doctoral candidate

_____

Print copies of the selected publications

MR elastography detection of early viscoelastic response of the murine hippocampus to amyloid β accumulation and neuronal cell loss due to Alzheimer's disease.
Munder T1, Pfeffer A1, Schreyer S1, Guo J2, Braun J3, Sack I2, Steiner B1, Klein C1.
J Magn Reson Imaging. 2018 Jan;47(1):105-114. Epub 2017 Apr 19.

https://doi.org/10.1002/jmri.25741

PLOS ONE

RESEARCH ARTICLE

Dopaminergic Neurodegeneration in the Mouse Is Associated with Decrease of Viscoelasticity of Substantia Nigra Tissue

Elisabeth G. Hain[1], Charlotte Klein[1], Tonia Munder[1], Juergen Braun[2], Kerstin Riek[3], Susanne Mueller[4], Ingolf Sack[3], Barbara Steiner[1]*

1 Department of Neurology, Charité, University Medicine Berlin, Berlin, Germany, **2** Institute for Medical Informatics, Charité, University Medicine Berlin, Berlin, Germany, **3** Department of Radiology, Charité, University Medicine Berlin, Berlin, Germany, **4** Center for Stroke Research Berlin, Berlin, Germany

* barbara.steiner@charite.de

Citation: Hain EG, Klein C, Munder T, Braun J, Riek K, Mueller S, et al. (2016) Dopaminergic Neurodegeneration in the Mouse Is Associated with Decrease of Viscoelasticity of Substantia Nigra Tissue. PLoS ONE 11(8): e0161179. doi:10.1371/journal.pone.0161179

Editor: Huaibin Cai, National Institutes of Health, UNITED STATES

Received: February 18, 2016

Accepted: August 1, 2016

Published: August 15, 2016

Data Availability Statement: All relevant data are within the paper and its Supporting Information files.

Funding: This study was funded by the German Research Foundation (www.dfg.de) to Barbara Steiner: STE 1450/8, and Ingolf Sack: SA901/17. The funder had no role in study design, data collection and analysis, decision to publish, or preparation of the manuscript.

Competing Interests: The authors have declared that no competing interests exist.

Abstract

The biomechanical properties of brain tissue are altered by histopathological changes due to neurodegenerative diseases like Parkinson's disease (PD). Such alterations can be measured by magnetic resonance elastography (MRE) as a non-invasive technique to determine viscoelastic parameters of the brain. Until now, the correlation between histopathological mechanisms and observed alterations in tissue viscoelasticity in neurodegenerative diseases is still not completely understood. Thus, the objective of this study was to evaluate (1) the validity of MRE to detect viscoelastic changes in small and specific brain regions: the substantia nigra (SN), midbrain and hippocampus in a mouse model of PD, and (2) if the induced dopaminergic neurodegeneration and inflammation in the SN is reflected by local changes in viscoelasticity. Therefore, MRE measurements of the SN, midbrain and hippocampus were performed in adult female mice before and at five time points after 1-methyl-4-phenyl-1,2,3,6-tetrahydropyridin hydrochloride (MPTP) treatment specifically lesioning dopaminergic neurons in the SN. At each time point, additional mice were utilized for histological analysis of the SN. After treatment cessation, we observed opposed viscoelastic changes in the midbrain, hippocampus and SN with the midbrain showing a gradual rise and the hippocampus a distinct transient increase of viscous and elastic parameters, while viscosity and–to a lesser extent—elasticity in the SN decreased over time. The decrease in viscosity and elasticity in the SN was paralleled by a reduced number of neurons due to the MPTP-induced neurodegeneration. In conclusion, MRE is highly sensitive to detect local viscoelastic changes in specific and even small brain regions. Moreover, we confirmed that neuronal cells likely constitute the backbone of the adult brain mainly accounting for its viscoelasticity. Therefore, MRE could be established as a new potential instrument for clinical evaluation and diagnostics of neurodegenerative diseases.

Introduction

The macroscopic biomechanical properties of *in vivo* brain tissue are influenced by the cellular composition of the brain given by the number of neurons and glial cells as well as their interactions with the extracellular matrix [1–3]. This composition varies in diverse brain regions and under pathological conditions so that histological differences may be reflected in the biomechanical properties of tissue and can be represented in viscoelastic quantities. Therefore, alterations in viscoelasticity can be considered to be a potential instrument for clinical evaluation and diagnostics.

Magnetic resonance elastography (MRE) attracted attention as an appropriate medical imaging technique to assess biomechanical properties of brain tissue non-invasively and *in vivo* [4]. Biomechanical constants of soft tissues are measured by inducing shear waves and processing the MR images of the propagating shear waves to calculate quantitative values of viscoelasticity such as the complex shear modulus G^* [4,5]. G^* contains the storage modulus G' and the loss modulus G''. G' gives information about the elasticity of the tissue, which is determined by the number and type of cells in the network. In contrast, G'' gives information about the viscous, dampening properties of the tissue, which depend on the geometry of the network including bonds and branching.

In human MRE studies, it has been found that brain viscoelasticity is reduced during aging [6,7] and under pathological conditions like multiple sclerosis (MS) [8,9], normal pressure hydrocephalus [10], Alzheimer's disease (AD) [11], frontotemporal dementia [12], Glioblastoma [13] and progressive supranuclear palsy [14]. However, the histopathological mechanisms underlying the observed alterations in tissue viscoelasticity are still not completely understood.

With the use of animal models, first steps have been made to elucidate the link between MRE parameters and histology. Millward, Riek and colleagues revealed a correlation between the degree of inflammation, mediated by T-cells and macrophages/microglia, and the viscoelastic constants in a mouse model of MS [15,16]. Schregel and co-workers underlined the decrease of elasticity in a different MS mouse model caused by demyelination and changed extracellular matrix configuration [3].

Aside from inflammation, neuronal alterations have also been observed to play an important role in changed viscoelastic parameters in the MRE. After middle cerebral artery occlusion in mice, the depleted density of neurons correlated directly with reduced elastic properties in the affected brain hemisphere [17]. In addition, mouse models for AD and Parkinson's disease (PD), have been investigated as well. A softening of brain tissue has been observed by MRE in APP-PS1 AD mice [18], but correlating histopathological analyses with particular regard to local changes correlating to region specific changes in MRE are missing. Changes in viscoelasticity and correlating histopathological mechanisms have been observed in previous animal studies in the whole brain [16], in one hemisphere [17] or the cerebellum [15], whereas such investigations in smaller brain regions are still not completed. In the 1-methyl-4-phenyl-1,2,3,6-tetrahydropyridine hydrochloride (MPTP) mouse model reproducing PD-like histopathology, a transient rise in viscoelasticity in the hippocampus has been observed. This was paralleled by a higher density of newly generated neurons, arising from a reactively generated precursor cell population [1]. However, the lesioned substantia nigra (SN) as the mainly affected structure in PD and its models has not been investigated yet in detail. In the work of Klein et al., basic principles in the relation between changes in the number of neurons under neurodegenerative conditions and MRE-measured viscoelastic properties using the MPTP mouse model for PD has been established [1].

PD, however, is initially and mainly characterized by the loss of dopaminergic neurons in the SN, a small region in the midbrain with synaptic connections to the surrounding basal

ganglia and beyond [19]. The neurotoxin MPTP is an established animal model for the histopathology seen in PD patients [20] due to its ability to selectively lesion dopaminergic cells in the SN, which is also accompanied by inflammatory reactions [21,22]. Up to now, Lipp and coworkers demonstrated a reduction of elasticity in the lentiform nucleus as part of the midbrain in humans with PD, whereas the viscoelastic properties of the whole brain were unaffected [14]. However, region specific changes of viscoelasticity due to aging and pathological conditions like neurodegenerative diseases and the analysis of underlying histopathological alterations is still lacking. Thus, we applied the MRE setup to MPTP-lesioned mice to investigate, if acquired viscoelastic parameters are altered in affected areas: the SN, midbrain and hippocampus. Furthermore, we investigated, if changes in MRE parameters in the SN correlate with neurodegenerative and inflammatory processes and if we can confirm that MRE is feasible to selectively detect local pathological alterations in neurodegenerative diseases. This would add to the establishment of MRE as clinical evaluation tool.

Materials and Methods

Animal Treatment

All animal experiments were approved by the local animal ethics committee (Landesamt für Gesundheit und Soziales, Berlin, Germany) and carried out in accordance with the European Communities Council directive of 22 September 2010 (10/63/EU). In total, 35 female eight to ten weeks old C57Bl/6N mice were group-housed in a temperature- and humidity-controlled colony room with a light/dark cycle of 12/12 h and unrestricted access to food and water.

Animals were randomly divided into seven groups of n = 5. All animals, except the histological counterparts for the baseline measurement, were treated intraperitoneally with MPTP (Sigma Aldrich, Steinheim, Germany), dissolved in 0.9% NaCl, with a concentration of 20 mg/kg bodyweight on three consecutive days. One group (n = 5) underwent MRE-imaging the day before MPTP treatment started (-3 days post-injection (dpi)) as baseline and three, six, ten, 14 and 18 days after the last MPTP injection (3, 6, 10, 14, 18dpi). At each time point (six in total), animals of the corresponding histological group (n = 5 for each time point) were perfused. A timeline of the experimental procedure is given in Fig 1 and Table 1.

Perfusion and Tissue Preparation

At each time point of MRE measurement, the corresponding histological group of animals were deeply anaesthetized with Ketamine/Xylacine (10% Ketamine hydrochloride, WDT; 2% Rompun, Provet AG) and transcardially perfused with phosphate buffered saline (PBS) and 4% paraformaldehyde (PFA). Brains were dissected carefully, postfixed in 4% PFA for 24 h and dehydrated with 30% sucrose solution for 48 h. Then they were frozen in 2-methylbutane (Sigma-Aldrich, Steinheim, Germany) cooled with liquid nitrogen, sliced in 40 μm thick coronal sections using a Leica CM 1850 UV cryostat and stored in cryoprotectant solution until histological stainings were performed.

Immunohistochemistry

For immunohistochemistry, a well-established staining protocol was followed [23,24]. Briefly, a one-in-six free-floating brain section series of each mouse was pre-treated with 0.6% H_2O_2 and donkey serum-enriched PBS (PBS+) before being incubated with the first antibody anti-Tyrosinhydroxylase (TH; mouse 1:10000, Sigma-Aldrich) or anti-ionized calcium-binding adapter molecule 1 (Iba-1; rat 1:1000, Wako) at 4°C overnight. On the next day, brain sections were first pre-treated with PBS+ for background blocking and then incubated with the

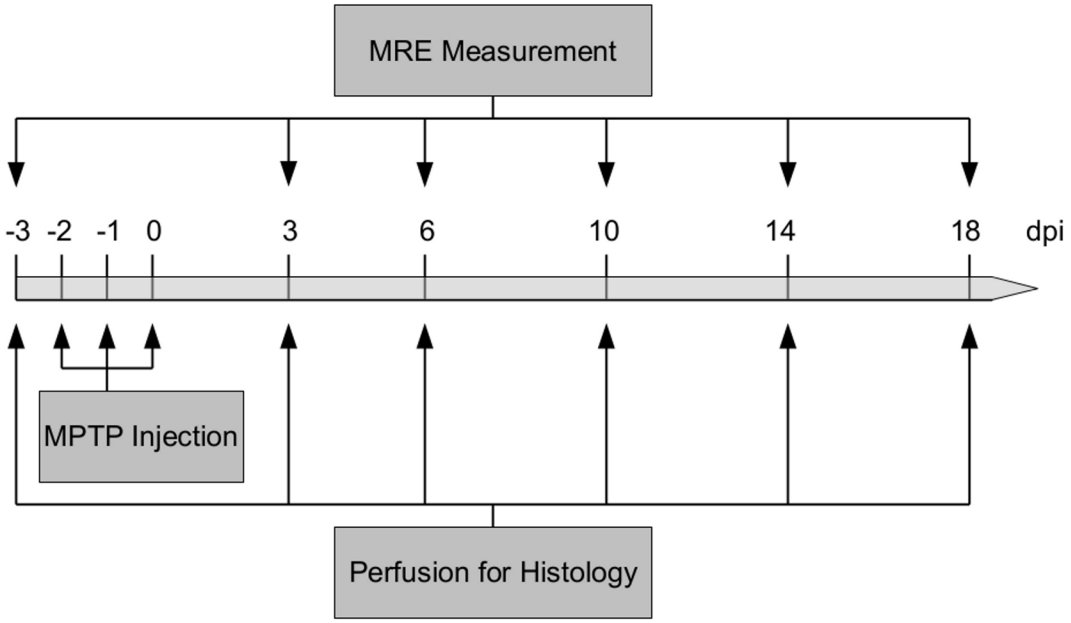

Fig 1. Timeline of the experimental procedure. The timeline of MPTP injections, time points of MRE measurement and brain perfusions for histological analyses.

doi:10.1371/journal.pone.0161179.g001

secondary biotinylated antibody (anti-mouse or anti-rat, 1:250, Dianova) at room temperature for two hours. Then, ABC solution (Vectastain Elite ABC Kit, Vector Laboratories) was applied, before the formed streptavidin-peroxidase complex was visualized by 3,3'-diaminobenzidine (DAB, Sigma-Aldrich)-nickel staining. Finally, stained sections were mounted on microscope slides and coverslipped.

To determine the total cell number in each region of interest (SN, midbrain and hippocampus), a separate one-in-twelve series of brain sections of two mice per group was stained with the fluorochrome 4',6-diamidino-2-phenylindole (DAPI), which binds to the DNA thereby labeling cell nuclei. Sections were incubated with PBS-diluted DAPI (1:1000, Thermo Scientific) for 7 min and afterwards mounted on microscope slides and coverslipped.

Cell Quantification

In total, four stained brain slices of each mouse were analyzed for TH+ cells in the SN, including pars compacta and pars reticulata. Cells were manually counted under the 40x objective of

Table 1. Experimental design.

Post-injection day	Performance
-3	MRE measurement or perfusion for histology
-2	MPTP injection
-1	MPTP injection
0	MPTP injection
3	MRE measurement or perfusion for histology
6	MRE measurement or perfusion for histology
10	MRE measurement or perfusion for histology
14	MRE measurement or perfusion for histology
18	MRE measurement or perfusion for histology

doi:10.1371/journal.pone.0161179.t001

an Axioskop HB50/AC light microscope (Zeiss, Germany) and multiplied by six to obtain an estimated absolute number of cells per SN.

For quantification of DAPI-stained cell nuclei in all regions of interest and Iba-1+ cells in the SN, the Stereo Investigator (MBF Bioscience) and a Leica DMRE microscope were used. The region of interest was defined with the 5x objective. Actual counting was done with the 40x oil objective. For quantification of DAPI-stained cell nuclei, two sections in an interval of twelve were counted by using a sampling grid size of 250x200 μm in the SN and 600x600μm in the midbrain and hippocampus. Iba-1 positive cells were counted in four sections in an interval of six by using a sampling grid size of 150x120 μm. In all brain regions, a counting frame of 60x60 μm without guard dissector height was used. Cells were counted when cell bodies became sharp in their widest extent. The absolute number of cells per brain regionwas automatically calculated based on the counted cell number, slice interval, counting frame size, sampling grid size and slice thickness.

Magnetic Resonance Elastography (MRE)

All measurements were realized on a 7-Tesla MR Imaging (MRI) scanner (Bruker PharmaScan 70/16, Ettlingen, Germany) with a 20 mm diameter 1H-RF-quadrature mouse head coil and using ParaVision 4.0 software. As illustrated in Fig 2, shear waves into the mouse brain were induced by using a moveable bite bar transducer, linked with a carbon fiber piston to an electromagnetic coil as the source of vibration. During the MRE session, mice were anaesthetized with isoflurane/oxygen. The transducer was gimballed through a rubber bearing and retaining bracket at the temperature-controlled mouse bed. This setup was held in the middle of the magnet bore of the MRI scanner by a plastic disc. Vibrations were induced by applying a sinusoidal electric current of 900 Hz frequency to an air-cooled Lorentz coil in the fringe area of the MRI scanner and were initialized by a trigger pulse from the control unit of the scanner, while the timing was defined by a customized FLASH sequence. Frequency, amplitude and number of sinusoidal oscillation cycles were controlled by an arbitrary function generator connected via an audio amplifier to the driving coil. The main polarization of the vibration was transverse to the principal axis of the magnet field, with amplitudes in the order of tens of micrometers.

The MRE data were acquired in one 2 mm transverse slice in which all regions of interests (ROI) could be analyzed. The imaging sequence was modified for MRE by sinusoidal motion sensitizing gradient (MSG) in the through-plane direction, as described elsewhere [16]. The MSG strength was 285 mT/m with a frequency of 900 Hz and nine periods. Phase difference images were calculated from two images differing in the sign of the MSG to compensate for static phase contributions. Additional imaging parameters were: a 128x128 matrix, 25 mm FoV, 14.3 ms echo time, 116.2 ms repetition time, eight dynamic scans over a vibration period and an acquisition time of 20 min.

Complex wave images according to the harmonic drive frequency were estimated by temporal Fourier transformation of the unfolded phase-difference images and filtered for suppressing noise and compression wave components [16,25]. An algebraic Helmholtz inversion was applied to the pre-processed 2D scalar wave fields calculating the complex shear modulus G^* [26]. Then, G^* was spatially averaged over the SN, midbrain and hippocampus of both hemispheres as ROIs, which were manually segmented by delineating its anatomical structure from T1w-MR images (Fig 3). Values of the averaged G^* contain the real part of G^*: storage modulus G', and the imaginary part of G^*: loss modulus G'', representing the elasticity and viscosity of tissue, respectively.

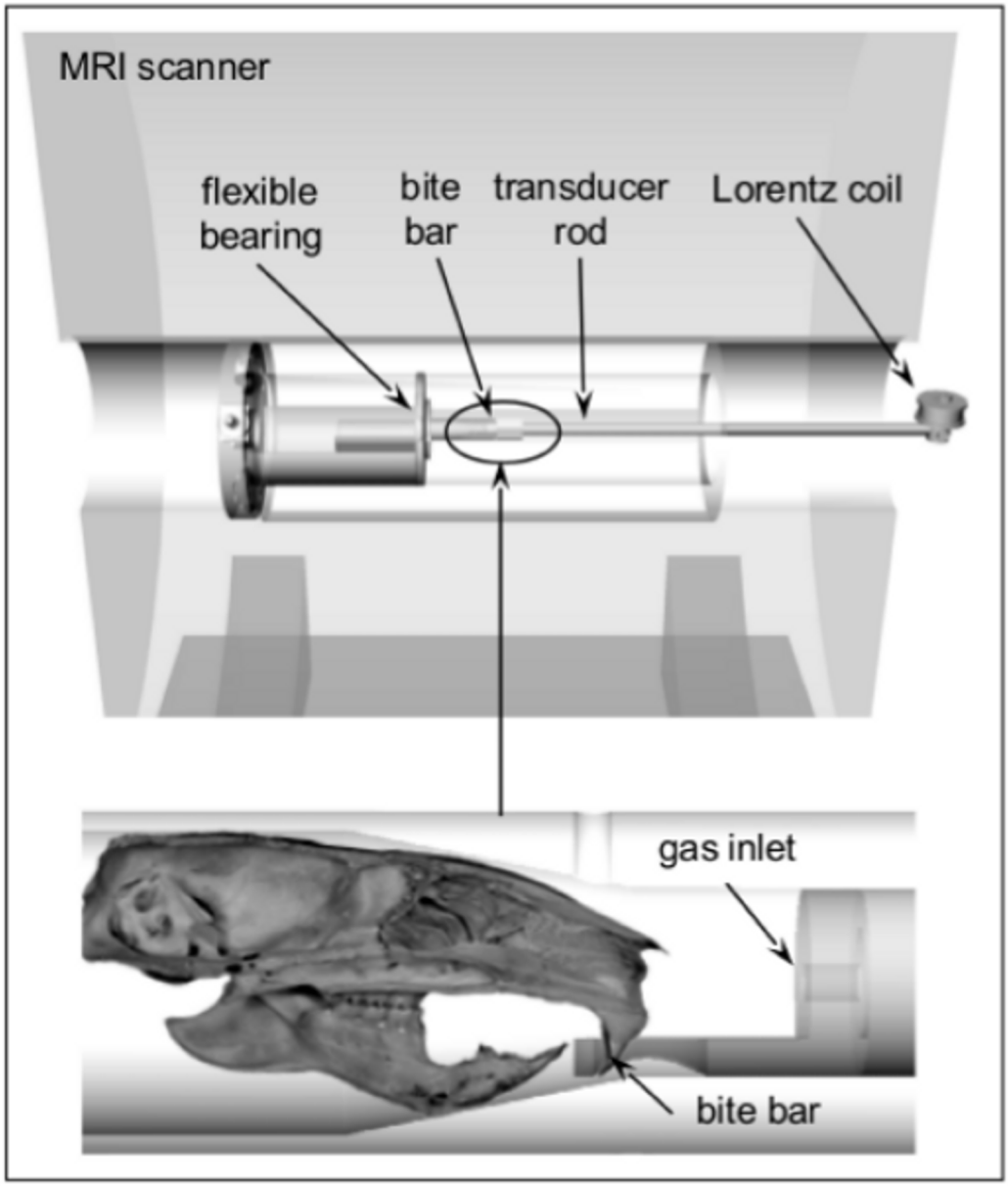

Fig 2. Schematic of the mouse MRE apparatus.

doi:10.1371/journal.pone.0161179.g002

Statistical Analysis

All statistical analyses were performed by using SPSS Statistics19 for Windows and GraphPad Prism 5. The homogeneity of variance was tested by Levene test. One-way ANOVA was performed the data from the quantification of TH+ and Iba1+ cells and one-way repeated measures (RM) ANOVA for MRE data. The data from the DAPI counts were not statistically evaluated, because only n = 2 per time point were quantified. Pairwise comparisons were done using the Bonferroni test in case of a significant ANOVA. The level of statistical significance was set at $p \leq 0.05$. All data are shown as mean values with standard error of the mean (SEM). Graphs were generated using GraphPad Prism 5.

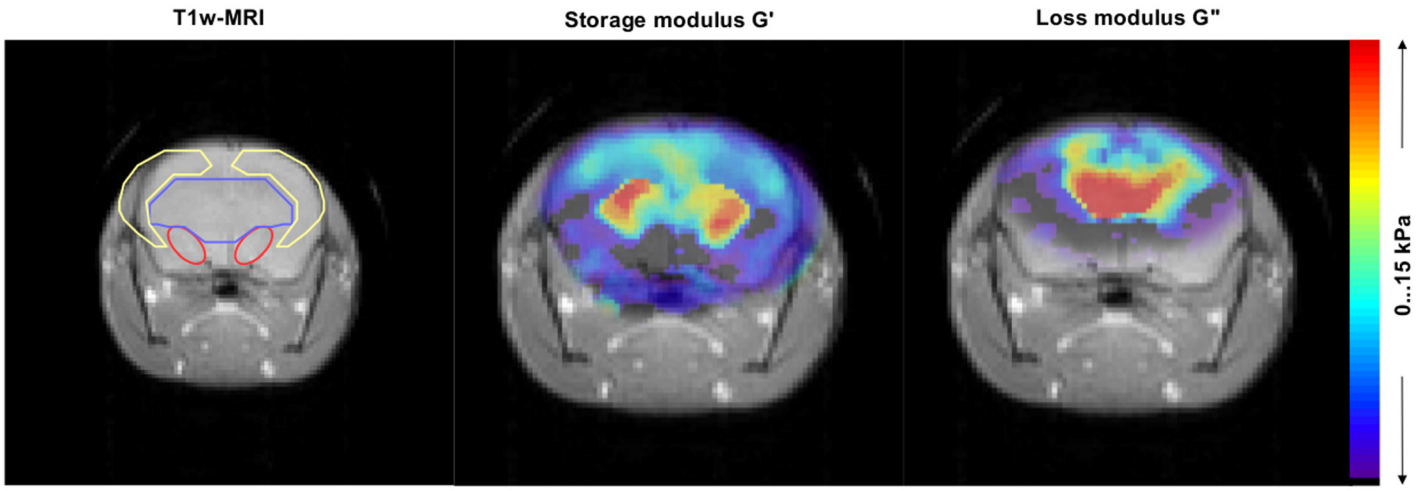

Fig 3. Representative images of MRI signal and complex modulus map of G' and G". Regions of interest: substantia nigra (red line), midbrain (blue line) and hippocampus (yellow line) were marked in T1w-MRI.

doi:10.1371/journal.pone.0161179.g003

Results

Initially, MRE measurement was performed the day before MPTP treatment started to generate baseline data of healthy brain tissue. Sessions were repeated three, six, ten, 14 and 18 days after the last MPTP injection and processed for the SN, midbrain and hippocampus. The MRE results are presented together with the results of the histological analysis of each brain region in Figs 4, 5 and 6.

One-way ANOVA of the MRE parameters at -3dpi revealed a significant difference in basic viscosity between the various brain areas ($F(2,14) = 5.396$, $p \leq 0.05$). Post-hoc pairwise comparison using the Bonferroni test showed a significant higher viscosity in the midbrain (1.836 ±0.043 kPa) than in the hippocampus (1.426 ±0.051 kPa) ($p \leq 0.05$).

MPTP induces a decrease of viscosity and elasticity in the SN

In the SN, MRE generated baseline values with mean (±SEM) of 5.012 (±0.578) kPa and 1.627 (±0.137) kPa for G' and G", respectively. A one-way RM ANOVA revealed a significant effect in the storage modulus G' ($F(5,29) = 4.274$, $p \leq 0.01$) and loss modulus G' ($F(5,29) = 8.350$, $p \leq 0.001$) following MPTP treatment, which reflects alterations in the elastic and viscous properties of the SN. Post-hoc pairwise comparison using the Bonferroni test showed a significant decrease in G' (3dpi vs. 6dpi: $p \leq 0.05$) (Fig 4a) and G" (-3dpi vs. 10dpi: $p \leq 0.05$, -3dpi vs. 18dpi: $p \leq 0.01$, -3dpi vs. 6dpi: $p \leq 0.001$) (Fig 4b), indicating a more reduced viscosity than elasticity in the SN following MPTP treatment with a slight restoration over time.

MPTP induces an increase of viscosity and elasticity in the midbrain

Mean values (±SEM) of G' and G" were 5.397 (±0.190) kPa and 1.836 (±0.043) kPa in the midbrain at -3dpi. The one-way RM ANOVA revealed a significant effect of MPTP treatment on storage modulus G' ($F(5,29) = 6.702$, $p \leq 0.001$) and loss modulus G' ($F(5,29) = 6.895$, $p \leq 0.001$) in the midbrain over time. A significant increase in G' (-3dpi vs. 14dpi: $p \leq 0.05$, -3dpi vs. 6dpi and 18dpi: $p \leq 0.01$) (Fig 5a) and G" (-3dpi vs. 6dpi and 18dpi: $p \leq 0.01$) (Fig 5b) was observed as the post-hoc pairwise comparison showed. This indicates tissue stiffening in the midbrain after MPTP treatment.

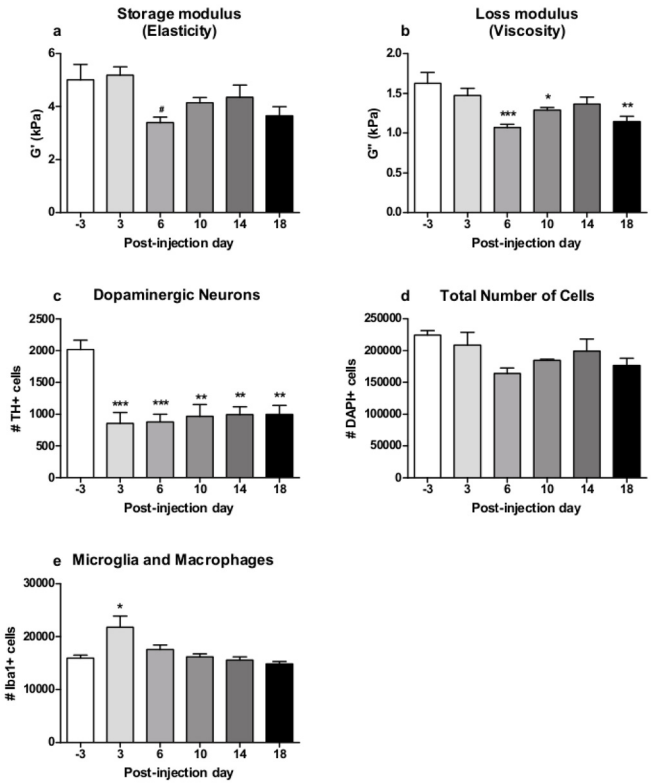

Fig 4. Results of MRE measurements and histological cell counts in the substantia nigra. MPTP induced a significant reduction in MRE elasticity (a) and viscosity (b) in the substantia nigra (mean±SEM, n (-3,3,6,10,14,18dpi) = 5). DAB-stained brain sections showed an immediate significant drop in TH+ dopaminergic neurons in the substantia nigra after MPTP treatment (c) (mean±SEM, n(-3dpi) = 4, n (3,6,10,14,18dpi) = 5). DAPI-stained cell amount was decreased by MPTP (d) (mean±SEM, n (-3,3,6,10,14,18dpi) = 2, no statistical analysis). Initially, the amount of Iba1+ microglia and macrophages was significantly raised after MPTP treatment, but ceased over time (e) (mean±SEM, n(-3dpi) = 4, n (3,6,10,14,18dpi) = 5). * vs. -3dpi, *$p \leq 0.05$, **$p \leq 0.01$, ***$p \leq 0.001$. # vs. 3dpi, # $p \leq 0.05$.

doi:10.1371/journal.pone.0161179.g004

MPTP induces a transient increase of viscosity and elasticity in the hippocampus

At baseline, mean values (±SEM) were 4.997 (±0.402) kPa and 1.426 (±0.52) kPa for G' and G'', respectively. The One-way RM ANOVA showed a significant effect of MPTP treatment on the storage modulus G' ($F(5,29) = 11.75$, $p \leq 0.001$) and loss modulus G' ($F(5,29) = 8.075$, $p \leq 0.001$) in the hippocampus over time. Here, post-hoc pairwise comparison revealed a significant increase in G' (-3dpi vs. 6dpi: $p \leq 0.001$) (Fig 6a) and G'' (-3dpi vs.6dpi: $p \leq 0.01$) (Fig 6b), indicating a transient tissue stiffening in the hippocampus six days after treatment cessation.

MPTP induces dopaminergic neurodegeneration in the SN

A one-way ANOVA revealed a strong effect of MPTP treatment on the number of TH+ in the SN ($F(5,28) = 7.499$, $p \leq 0.001$). Pairwise comparison showed that the number of TH+ dopaminergic neurons was decreased by MPTP at all time points in comparison to baseline level (-3dpi vs. 3dpi and 6dpi: $p \leq 0.001$, -3dpi vs. 10dpi, 14dpi and 18dpi: $p \leq 0.01$) (Fig 4c). The immediate reduction of TH+ dopaminergic neurons following MPTP treatment was approximately 57% with mean values declining from 2018 at -3dpi to 856 at 3dpi, respectively. The deficit of dopaminergic neurons persisted at least until the last time point at 18dpi investigated

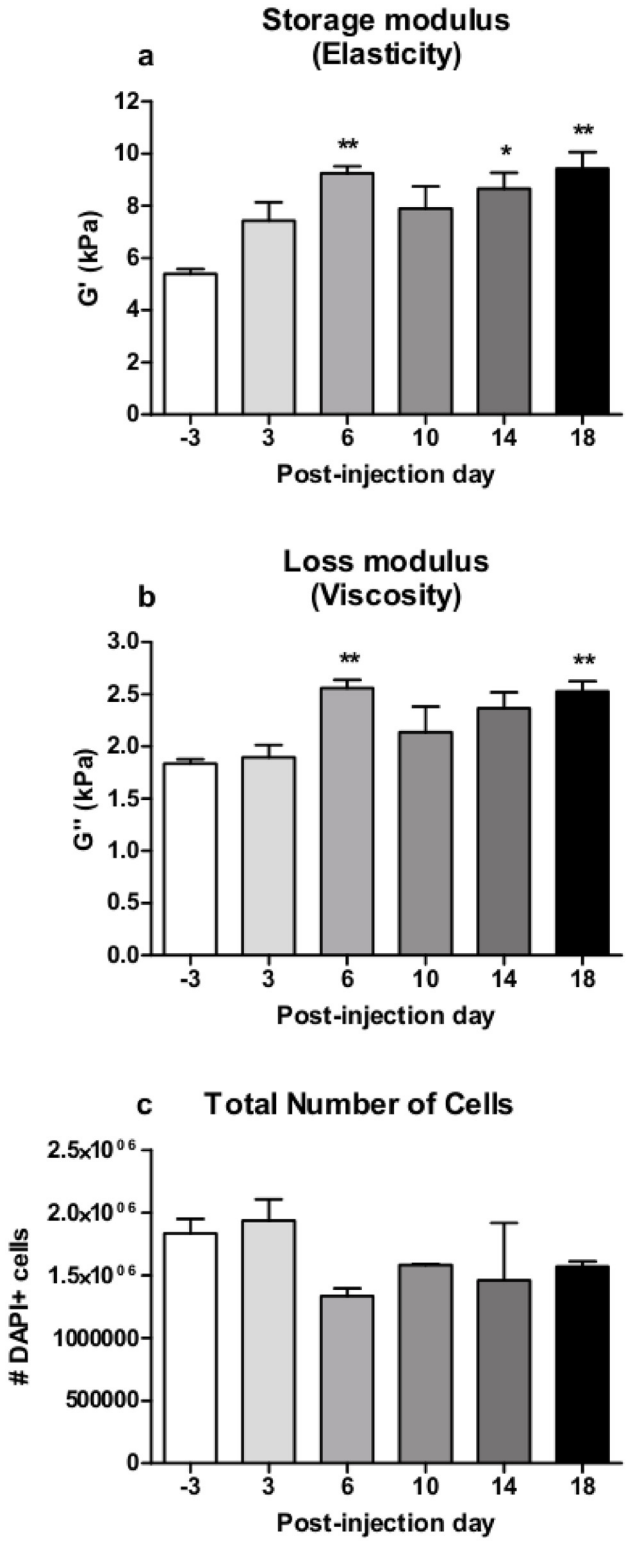

Fig 5. Results of MRE measurement and histological cell count in the midbrain. MPTP induced a significant increase of MRE elasticity (a) and viscosity (b) in the midbrain (mean±SEM, n (-3,3,6,10,14,18dpi = 5). DAPI-stained brain sections showed a reduction following MPTP-treatment (c) (mean±SEM, n(-3,3,6,10,14,18dpi) = 2, no statistical analysis). * vs. -3dpi, *p≤0.05, **p≤0.01.

doi:10.1371/journal.pone.0161179.g005

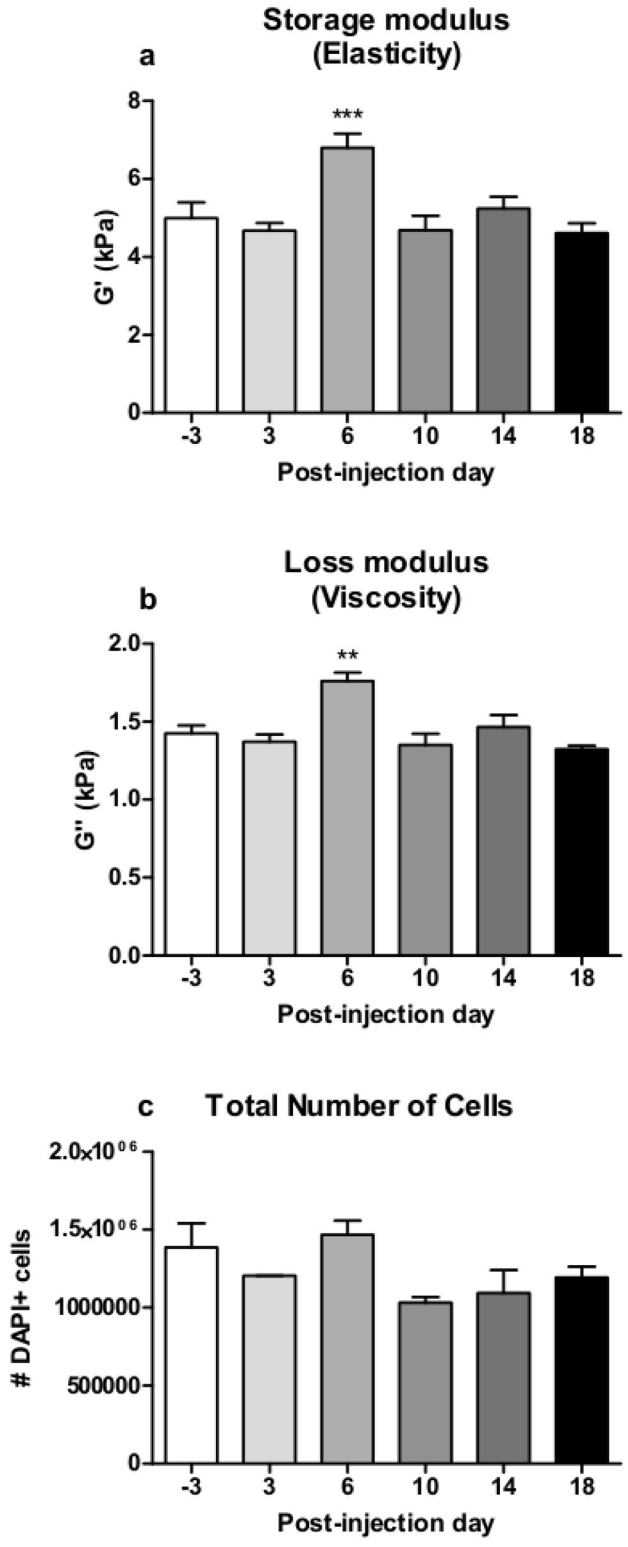

Fig 6. Results of MRE measurement and histological cell count in the hippocampus. MPTP induced a transient increase of elasticity (a) and viscosity (b) in the hippocampus at 6dpi (mean±SEM, n (-3,3,6,10,14,18dpi = 5). Quantification of DAPI-stained cells showed an elevated amount at 6dpi (mean ±SEM, n(-3,3,6,10,14,18dpi) = 2, no statistical analysis). * vs. -3dpi, **$p \leq 0.01$, ***$p \leq 0.001$.

doi:10.1371/journal.pone.0161179.g006

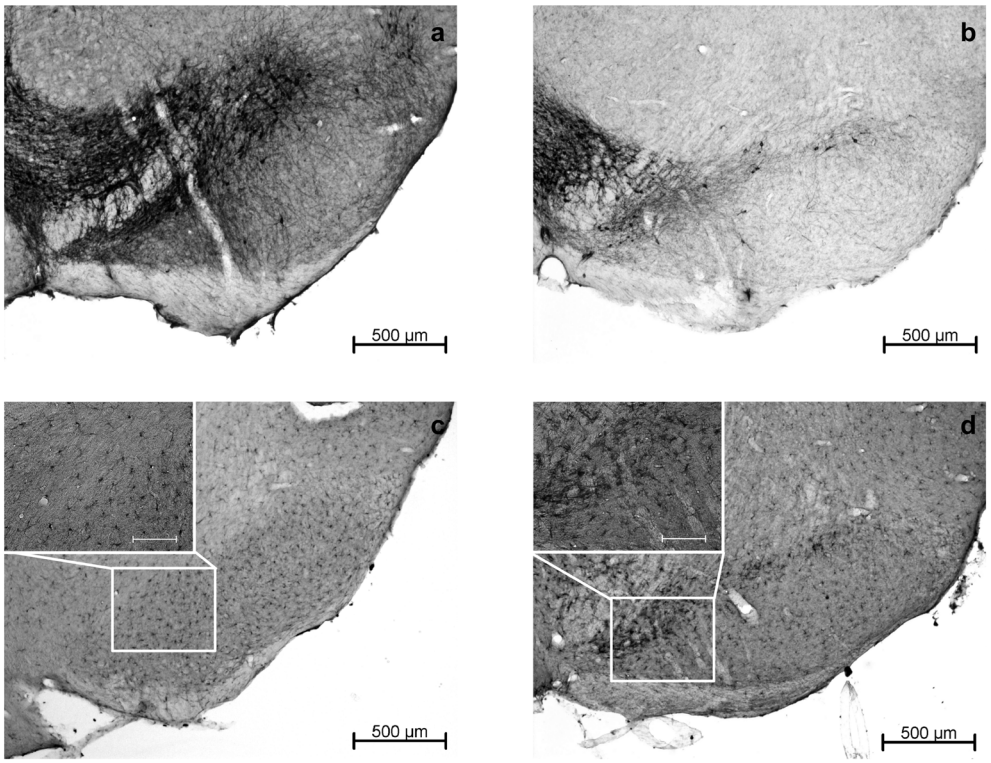

Fig 7. Representative images of DAB–stained brain slices showing the substantia nigra. TH+ cells at baseline at -3dpi (a) and directly after MPTP treatment at 3dpi (b) at 50x magnification, indicating a severe loss of dopaminergic neurons induced by MPTP. Iba-1+ at -3dpi (c) and 3dpi (d) at 50x magnification with detail in 200x magnification (scale bar 100 µm), showing a reactive increase in the number of microglia and macrophages in the substantia nigra immediately after MPTP treatment.

doi:10.1371/journal.pone.0161179.g007

here. Representative images of TH+ cells before and after MPTP treatment are shown in Fig 7a and 7b.

MPTP induces a reduction of total cell amount in the SN and midbrain and a transient rise in the hippocampus

In the SN, the quantification of DAPI+ cells (n = 2) revealed a decrease in the total amount of cells from 224700 (±6967) cells at -3dpi to 164083 (±8417) cells at 6dpi following MPTP-treatment. After that, a transient slight restoration over time can be observed (Fig 4d).

The DAPI+ cell count (n = 2) in the midbrain revealed a decrease in the total cell amount from 1834800 (±116400) to 1333800 (±60600) cells at -6dpi (Fig 5c).

In the hippocampus, the DAPI+ cell quantification (n = 2) revealed a total amount of 1385400 (±155400) cells at -3dpi and a transient rise at 6dpi up to 1468200 (±89400) cells (Fig 6c).

MPTP induces a transient increase of microglia and macrophages in the SN

The analysis of Iba1+ cell counts revealed a significant effect of MPTP treatment on the number of microglia and macrophages in the SN as a sign for a local inflammatory reaction ($F(5,28) = 5.706$, $p \leq 0.01$). Pairwise comparison showed that the amount of Iba+ cells directly after MPTP treatment (3dpi) was significantly higher than at baseline (-3dpi vs. 3dpi: $p \leq 0.05$), whereas no significant difference in the amount of Iba-1+ cells was observed between baseline

and later time points from 6dpi to the end of the study (Fig 4d). MPTP induced a transient inflammatory response, which is reflected here by increased numbers of microglia in the SN at 3dpi (21732 cells), that ceased over time until baseline levels (approximately 15000 cells) are reached again at 18dpi. Representative images of Iba+ cells before and after MPTP treatment are shown in Fig 7c and 7d.

Discussion

In this study, we demonstrate how viscosity and elasticity in various brain areas change in response to MPTP treatment and that the significant reduction of dopaminergic neurons in the SN in a mouse model for a neurodegenerative disease is reflected in the decrease of viscosity and–to a lesser extent–elasticity. Hence, the MRE setup is viable to detect viscous and elastic alterations even in small brain areas.

The neurotoxin MPTP primarily affects dopaminergic neurons and is therefore an established animal model for the histopathology seen in PD patients [19,20]. Besides the SN, the MPTP mouse model is also used for investigations in the midbrain [27] and hippocampus [24] to elucidate the effects of nigral dopaminergic neurodegeneration in other specific brain regions related to the pathology of PD. According to the fact that PD (and its animal model) includes the neurodegenerative affection of different areas in the brain, e.g. reduced neural precursor cells caused by dopamine denervation in the subgranular zone of the hippocampus [28], such extra-nigral histopathological changes were correlated to region specific changes in viscoelasticity detected by MRE [1].

In the SN, we observed a significant decrease in viscosity and–to a lesser extent—elasticity six days after treatment cessation followed by a slight but non-significant restoration over time. MPTP seem to primarily affect the geometry of the cellular network in the SN and secondarily the cell density. This is comprehensible considering the structure of the SN, with dopaminergic cell bodies and many cellular processes, which are substantially reduced after MPTP treatment (see Fig 7a and 7b for comparison). Our findings are in line with an observed tissue softening in other animal and human studies of pathological conditions [8,15,17].

Surprisingly, in contrast to the SN, calculated MRE parameters of the midbrain were significantly higher after treatment compared to healthy baseline values. This rather indicates an increase in tissue stiffness in response to MPTP. The decreased total amount of DAPI+ cells does not correlate with this finding. Up to now, it is known that MPTP treatment does not lead to dopaminergic neurodegeneration in the midbrain in contrast to the SN [27]. The biomechanical properties of tissue are not only determined by individual cell types and cellular density but also by the complexity of the cellular network, which depends on the degree of cross-linking and branching, and the interaction with the extracellular matrix [1–3]. The discrepancy between midbrain MRE and histology data may therefore be attributed to other processes following MPTP treatment than the ones examined here, as the midbrain is a larger and more complex area with several core regions and white matter tracts than the SN and hippocampus and cannot be narrowed down to only neuronal cells. Though MRE sensitively detects local tissue alterations, the specificity of the method is not yet established in detail.

Interestingly, a higher basic viscosity was observed in the midbrain compared to the hippocampus in healthy yet untreated mice at -3dpi. As mentioned above, the midbrain tissue exhibits more complex network geometry with diverse core regions and white matter tracts. In humans, white matter has been shown to be stiffer than gray matter [29,30], which is in line with our observed higher viscosity in the midbrain.

In the hippocampus we observed a transient rise of the storage and loss modulus as described in our previous study [1]. In correlation to that, the total amount of cells was also

transiently elevated at 6dpi. This underlines the histological findings of Klein and colleagues, showing increased stiffness in the hippocampus following MPTP treatment. This was correlated to a higher percentage of newly generated neurons resulting from a reactively enhanced precursor cell proliferation [1].

The significant reduction of G' and G'' in the SN at 6dpi without full restoration over time is paralleled by the reduction of TH+ dopaminergic neurons. It is well-known that the neurotoxin MPTP damages dopaminergic neurons in the SN already shortly after application, which has been demonstrated by a reduced amount of TH+ cells [23,24,31]. In our study, we confirm the MPTP-induced decrease of TH activity in dopaminergic neurons of the SN. Although the amount of TH+ neurons is already significantly reduced three days after MPTP treatment, MRE parameters are changed not until 6dpi. Importantly, TH activity has been shown to decrease first, followed and paralleled by a "real" reduction in the number of neurons after MPTP treatment [32]. We confirm this observation by the quantified number of DAPI+ cells, which correlates with the changes in viscosity. This means that the changed loss and–to a lesser extent—storage modulus in our study are representative for the dopaminergic neurodegeneration in the SN. Moreover, our findings are in accordance with the hypothesis that a decrease of viscoelastic properties of the adult brain is mainly based on the reduced number of neuronal cells, which has first been investigated in a murine stoke model as an example of disturbed brain structure [17].

In line with a decreased brain stiffness in APP-PS1 mice, modelling AD [18], our results support the assumption that viscoelastic properties in neurodegenerative diseases decrease in the mainly affected area and can be correlated with histopathological changes in our animal model for PD. As investigated here, the neurotoxin MPTP leads to different viscous and elastic changes in adult mice depending on the studied brain area. Therefore, we conclude that alterations in MRE parameters following MPTP treatment are highly region-specific.

The size of the processed ROI in the SN is a relevant factor in our study. While in previous animal studies, MRE changes have been observed in the whole brain [16], in one hemisphere [17], in the hippocampus [1] or the cerebellum [15], we processed our MRE data from a smaller brain region. However, our correlating histological findings imply that the MRE setup is eligible to detect viscous and elastic alterations even in small brain areas such as the SN.

Besides dopamine depletion, MPTP provokes an inflammatory response. It has been shown, that the neurotoxin initially leads to a higher amount of microglia and oligodendrocytes in the SN and hippocampus, which diminishes over time after treatment cessation [1,21,23,33]. This course of inflammatory reaction in response to MPTP is also seen in our study. However, the initially elevated amount of Iba+ cells in the SN is not reflected in MRE parameters. Similar observations have been made before in the hippocampus by Klein et al. [1]. Thus, the present data suggest that MRE may not be suitable for detecting elevated amounts of microglia and macrophages or oligodendrocytes as a sign of a transient local inflammation at least with regard to particular structures as the SN and hippocampus. Therefore, the present data further support the hypothesis that neuronal cells likely constitute the mechanical backbone of the adult brain. However, the biomechanical properties of tissue not only depend on mere cell numbers of one neural cell type but also on other cell types, the network neural cells build by cross-linking and branching and their interaction with the extracellular matrix. Even though neuronal cells have been identified to playing a key role in viscoelasticity, important influence from other cell types, networks and interactions cannot be excluded.

In the present study, female mice were used. Human studies have revealed that female brains are stiffer than brains of age-matched male counterparts [7,9]. This raises the question, if the observed changes predominantly in the viscous properties of SN tissue following MPTP-induced neurodegeneration are stable across sex in mice or if differences as in the mentioned

human studies can be found. We have successfully established the MPTP mouse model in females to study the dopamine dependency of functional neurogenesis in the hippocampus and SN [23,24,34]. Thus, the present study can also be compared to our previous MRE study in MPTP-treated female mice [1].

In summary, we demonstrated the feasibility of MRE to sensitively detect viscoelastic changes in small and specific brain regions within an animal model for PD. Furthermore, we contribute to the investigation of the missing link between histopathological alterations and observed biomechanical constants in the SN, by demonstrating that changes in the amount of dopaminergic neurons in the SN of MPTP-lesioned mice are detectable by MRE. Thus, MRE is highly sensitive for the observation of local viscoelastic changes in particular brain regions adding to the understanding of how altered histopathological conditions influence biomechanical parameters of brain tissue that are changed under pathological conditions. This will help to establish MRE as a new potential instrument for clinical evaluation and diagnostics of neurodegenerative diseases.

Supporting Information

S1 Table. Results of MRE measurement in the substantia nigra, the midbrain and the hippocampus.
(PDF)

S2 Table. Results of histological cell count in the substantia nigra, the midbrain and the hippocampus.
(PDF)

Acknowledgments

We thank Jennifer Altschueler for technical assistance.

Author Contributions

Conceived and designed the experiments: EH CK KR IS BS.

Performed the experiments: EH CK TM KR SM.

Analyzed the data: EH CK JB IS.

Contributed reagents/materials/analysis tools: SM JB IS BS.

Wrote the paper: EH CK IS BS.

References

1. Klein C, Hain EG, Braun J, Riek K, Mueller S, Steiner B, et al. Enhanced adult neurogenesis increases brain stiffness: in vivo magnetic resonance elastography in a mouse model of dopamine depletion. PloS One 2014; 9: e92582. doi: 10.1371/journal.pone.0092582 PMID: 24667730
2. Lu Y-B, Iandiev I, Hollborn M, Körber N, Ulbricht E, Hirrlinger PG, et al. Reactive glial cells: increased stiffness correlates with increased intermediate filament expression. FASEB J. 2011; 25: 624–631. doi: 10.1096/fj.10-163790 PMID: 20974670
3. Schregel K, Wuerfel E, Garteiser P, Gemeinhardt I, Prozorovski T, Aktas O, et al. Demyelination reduces brain parenchymal stiffness quantified in vivo by magnetic resonance elastography. Proc Natl Acad Sci USA 2012; 109: 6650–6655. doi: 10.1073/pnas.1200151109 PMID: 22492966
4. Muthupillai R, Lomas DJ, Rossman PJ, Greenleaf JF, Manduca A, Ehman RL. Magnetic resonance elastography by direct visualization of propagating acoustic strain waves. Science 1995; 269: 1854–1857. PMID: 7569924

5. Mariappan YK, Glaser KJ, Ehman RL. Magnetic resonance elastography: a review. Clin Anat. 2010; 23: 497–511. doi: 10.1002/ca.21006 PMID: 20544947
6. Arani A, Murphy MC, Glaser KJ, Manduca A, Lake DS, Kruse SA, et al. Measuring the effects of aging and sex on regional brain stiffness with MR elastography in healthy older adults. Neuroimage 2015; 111: 59–64. doi: 10.1016/j.neuroimage.2015.02.016 PMID: 25698157
7. Sack I, Beierbach B, Wuerfel J, Klatt D, Hamhaber U, Papazoglou S, et al. The impact of aging and gender on brain viscoelasticity. Neuroimage 2009; 46: 652–657. doi: 10.1016/j.neuroimage.2009.02.040 PMID: 19281851
8. Streitberger KJ, Sack I, Krefting D, Pfueller C, Braun J, Paul F, et al. Brain viscoelasticity alteration in chronic-progressive multiple sclerosis. PloS One 2012; 7: e29888. doi: 10.1371/journal.pone.0029888 PMID: 22276134
9. Wuerfel J, Paul F, Beierbach B, Hamhaber U, Klatt D, Papazoglou S, et al. MR-elastography reveals degradation of tissue integrity in multiple sclerosis. Neuroimage 2010; 49: 2520–2525. doi: 10.1016/j.neuroimage.2009.06.018 PMID: 19539039
10. Streitberger KJ, Wiener E, Hoffmann J, Freimann FB, Klatt D, Braun J, et al. In vivo viscoelastic properties of the brain in normal pressure hydrocephalus. NMR Biomed. 2011; 24: 385–392. doi: 10.1002/nbm.1602 PMID: 20931563
11. Murphy MC, Huston J 3rd, Jack CR Jr, Glaser KJ, Manduca A, Felmlee JP, et al. Decreased brain stiffness in Alzheimer's disease determined by magnetic resonance elastography. J Magn Reson Imaging 2011; 34: 494–498. doi: 10.1002/jmri.22707 PMID: 21751286
12. Huston J 3rd, Murphy MC, Boeve BF, Fattahi N, Arani A, Glaser KJ, et al. Magnetic resonance elastography of frontotemporal dementia. J Magn Reson Imaging 2016; 43: 474–478. doi: 10.1002/jmri.24977 PMID: 26130216
13. Streitberger KJ, Reiss-Zimmermann M, Freimann FB, Bayerl S, Guo J, Arlt F, et al. High-resolution mechanical imaging of glioblastoma by multifrequency magnetic resonance elastography. PloS One 2014; 9: e110588. doi: 10.1371/journal.pone.0110588 PMID: 25338072
14. Lipp A, Trbojevic R, Paul F, Fehlner A, Hirsch S, Scheel M, et al. Cerebral magnetic resonance elastography in supranuclear palsy and idiopathic Parkinson's disease. Neuroimage Clin. 2013; 3: 381–387. doi: 10.1016/j.nicl.2013.09.006 PMID: 24273721
15. Millward JM, Guo J, Berndt D, Braun J, Sack I, Infante-Duarte C. Tissue structure and inflammatory processes shape viscoelastic properties of the mouse brain. NMR Biomed. 2015; 28: 831–839. doi: 10.1002/nbm.3319 PMID: 25963743
16. Riek K, Millward JM, Hamann I, Mueller S, Pfueller CF, Paul F, et al. Magnetic resonance elastography reveals altered brain viscoelasticity in experimental autoimmune encephalomyelitis. Neuroimage Clin. 2012; 1: 81–90. doi: 10.1016/j.nicl.2012.09.003 PMID: 24179740
17. Freimann FB, Mueller S, Streitberger KJ, Guo J, Rot S, Ghori A, et al. MR elastography in a murine stroke model reveals correlation of macroscopic viscoelastic properties of the brain with neuronal density. NMR Biomed. 2013; 26: 1534–1539. doi: 10.1002/nbm.2987 PMID: 23784982
18. Murphy MC, Curran GL, Glaser KJ, Rossman PJ, Huston J 3rd, Poduslo JF, et al. Magnetic resonance elastography of the brain in a mouse model of Alzheimer's disease: initial results. Magn Reson Imaging 2012; 30: 535–539. doi: 10.1016/j.mri.2011.12.019 PMID: 22326238
19. Hirsch E, Graybiel AM, Agid YA. Melanized dopaminergic neurons are differentially susceptible to degeneration in Parkinson's disease. Nature 1988; 334: 345–348. PMID: 2899295
20. Jackson-Lewis V, Przedborski S. Protocol for the MPTP mouse model of Parkinson's disease. Nat Protoc. 2007; 2: 141–151. PMID: 17401348
21. McGeer PL, McGeer EG. Glial reactions in Parkinson's disease. Mov Disord. 2008; 23: 474–483. PMID: 18044695
22. Przedborski S, Vila M. The 1-methyl-4-phenyl-1,2,3,6-tetrahydropyridine mouse model: a tool to explore the pathogenesis of Parkinson's disease. Ann N Y Acad Sci. 2003; 991: 189–198. PMID: 12846987
23. Klaissle P, Lesemann A, Huehnchen P, Hermann A, Storch A, Steiner B. Physical activity and environmental enrichment regulate the generation of neural precursors in the adult mouse substantia nigra in a dopamine-dependent manner. BMC Neurosci. 2012; 13: 132. doi: 10.1186/1471-2202-13-132 PMID: 23110504
24. Lesemann A, Reinel C, Huehnchen P, Pilhatsch M, Hellweg R, Klaissle P, et al. MPTP-induced hippocampal effects on serotonin, dopamine, neurotrophins, adult neurogenesis and depression-like behavior are partially influenced by fluoxetine in adult mice. Brain Res. 2012; 1457: 51–69. doi: 10.1016/j.brainres.2012.03.046 PMID: 22520437

25. Clayton EH, Garbow JR, Bayly PV. Frequency-depent viscoelastic parameters of mouse brain tissue estimated by MR elastography. Phys Med Biol. 2011; 56: 2391–2406. doi: 10.1088/0031-9155/56/8/005 PMID: 21427486

26. Papazoglou S, Hamhaber U, Braun J, Sack I. Algebraic Herlmholtz inversion in planar magnetic resonance elastography. Phys Med Biol. 2008; 53: 3147–3158. doi: 10.1088/0031-9155/53/12/005 PMID: 18495979

27. Phani S, Gonye G, Iacovitti L. VTA neurons show a potentially protective transcriptional response to MPTP. Brain Res. 2010; 343: 1–13.

28. Höglinger GU, Rizk P, Muriel MP, Duyckaerts C, Oertel WH, Caille I, et al. Dopamine depletion impairs precursor cell proliferation in Parkinson disease. Nat Neurosci. 2004; 7: 726–735. PMID: 15195095

29. Kruse SA, Rose GH, Glaser KJ, Manduca A, Felmlee P, Jack CR Jr, et al. Magnetic resonance elastography of the brain. NeuroImage. 2008; 39:231–237. PMID: 17913514

30. McCracken PJ, Manduca A, Felmlee J, Ehman RL. Mechanical transient-based magnetic resonance elastography. Magn Reson Med. 2005; 53:628–639. PMID: 15723406

31. Araki T, Mikami T, Tanji H, Matsubara M, Imai Y, Mizugaki M, et al. Biochemical and immunohistological changes in the brain of 1-methyl-4-phenyl-1,2,3,6-tetrahydropyridine (MPTP)-treated mouse. Eur J Pharm Sci. 2001; 12: 231–238. PMID: 11113642

32. Jackson-Lewis V, Jakowec M, Burke RE, Przedborski S. Time course and morphology of dopaminergic neuronal death caused by the neurotoxin 1-methyl-4-phenyl-1,2,3,6-tetrahydropyridine. Neurodegeneration 1995; 4: 257–269. PMID: 8581558

33. Annese V, Herrero MT, Di Pentima M, Gomez A, Lombardi L, Ros CM, et al. Metalloproteinase-9 contributes to inflammatory glia activation and nigro-striatal pathway degeneration in both mouse and monkey models of 1-methyl-4-phenyl-1,2,3,6-tetrahydropyridine (MPTP)-induced Parkinsonism. Brain Struct Funct. 2015; 220: 703–727. doi: 10.1007/s00429-014-0718-8 PMID: 24558048

34. Klein C, Rasińka J, Empl L, Sparenberg M, Poshtiban A, Hain EG et al. Physical exercise counteracts MPTP-induced changes in neural precursor cell proliferation in the hippocampus and restores spatial learning but not memory performance in the water maze. Behav Brain Res. 2016; 307: 227–238. doi: 10.1016/j.bbr.2016.02.040 PMID: 27012392

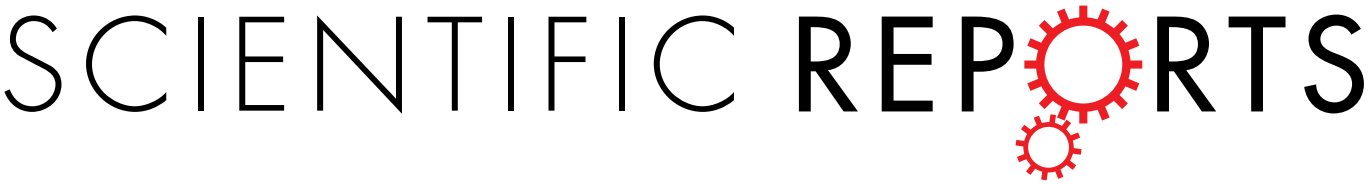

OPEN

Stimulation of adult hippocampal neurogenesis by physical exercise and enriched environment is disturbed in a CADASIL mouse model

Received: 29 November 2016
Accepted: 23 February 2017
Published: 27 March 2017

C. Klein, S. Schreyer, F. E. Kohrs, P. Elhamoury, A. Pfeffer, T. Munder & B. Steiner

In the course of CADASIL (Cerebral Autosomal Dominant Arteriopathy with Subcortical Infarcts and Leukoencephalopathy), a dysregulated adult hippocampal neurogenesis has been suggested as a potential mechanism for early cognitive decline. Previous work has shown that mice overexpressing wild type Notch3 and mice overexpressing Notch3 with a CADASIL mutation display impaired cell proliferation and survival of newly born hippocampal neurons prior to vascular abnormalities. Here, we aimed to elucidate how the long-term survival of these newly generated neurons is regulated by Notch3. Knowing that adult neurogenesis can be robustly stimulated by physical exercise and environmental enrichment, we also investigated the influence of such stimuli as potential therapeutic instruments for a dysregulated hippocampal neurogenesis in the CADASIL mouse model. Therefore, young-adult female mice were housed in standard (STD), environmentally enriched (ENR) or running wheel cages (RUN) for either 28 days or 6 months. Mice overexpressing mutated Notch3 and developing CADASIL ($TgN3^{R169C}$), and mice overexpressing wild type Notch3 ($TgN3^{WT}$) were used. We found that neurogenic stimulation by RUN and ENR is apparently impaired in both transgenic lines. The finding suggests that a disturbed neurogenic process due to Notch3-dependent micromilieu changes might be one vascular-independent mechanism contributing to cognitive decline observed in CADASIL.

Cerebral Autosomal Dominant Arteriopathy with Subcortical Infarcts and Leukoencephalopathy (CADASIL) is the most common heritable cause of stroke and vascular dementia in adults[1–3]. It represents a genetic archetype of non-hypertensive ischemic cerebral small vessel disease. CADASIL patients carry dominant mutations in the *notch3* gene, which encodes a transmembrane receptor belonging to the Notch receptor family. Notch3 is required for the structural and functional integrity of small arteries. It is predominantly expressed in vascular smooth muscle cells and pericytes, controlling their arterial differentiation and maturation[4,5]. The highly stereotyped mutations alter the number of cysteine residues in the extracellular domain of Notch3 ($Notch3^{ECD}$), leading to abnormal vascular accumulation of mutated $Notch3^{ECD}$[3]. In CADASIL, small and medium sized arteries characteristically exhibit pathognomonic deposits of granular osmiophilic material (GOM) containing mutated $Notch3^{ECD}$. The resulting progressive degeneration of vascular smooth muscle cells (vSMC) leads to arteriole dysfunction, followed by subcortical lacunes with white matter injury. Cortico-cortical network disruptions in the frontal lobe have also been recently reported[6]. White matter infarcts are usually considered the leading cause of the progressive decline in cognitive function[7]. However, CADASIL patients show a decline in cognitive function prior to any infarcts[8,9].

Interestingly, Notch3 has also been found to be expressed in neural precursor cells of the adult hippocampus[10]. Adult hippocampal neurogenesis is a lifelong process during which new neurons are generated in the subgranular zone (SGZ) and functionally integrated into neuronal networks[11,12]. This might represent a part of the CADASIL pathology as hippocampal neurogenesis has been demonstrated to play a crucial role in hippocampus-dependent learning and memory, maintaining cognitive flexibility during adulthood and ageing[13–15]. In general, Notch is a

Charité – University Medicine, Department of Neurology, Berlin, Germany. Correspondence and requests for materials should be addressed to B.S. (email: barbara.steiner@charite.de)

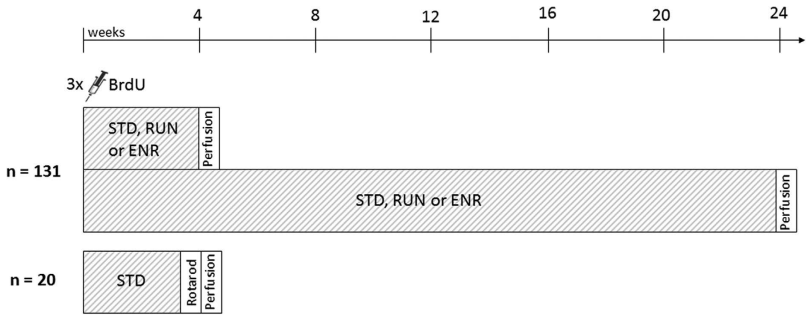

Figure 1. Experimental Design. Mice of each genotype were housed in standard (STD), running wheel (RUN) or enriched environment (ENR) cages for either a short (28 days) or a long duration (6 months).

key regulator in the crosstalk between neurogenesis and angiogenesis. It controls vessel sprouting and is required for proliferation and differentiation of stem and precursor cells[16–18]. Moreover, adult hippocampal neurogenesis occurs in a highly vascularized niche of the SGZ[19]. Here, capillaries provide the supply of nutrients and oxygen to maintain the proliferative capacity of the stem and precursor cells. As *notch3* mutations in CADASIL lead to arteriole dysfunction and decreased blood flow[20,21], it seems plausible that the resulting deficit in oxygen and glucose might influence adult hippocampal neurogenesis. Aside from the direct effect Notch3 can exert on neurogenesis by its expression in neural precursor cells, the Notch3-dependent vascular influence might, in turn, also be responsible for the observed cognitive impairments in CADASIL patients. Our previous study using a mouse model overexpressing Notch3 with a CADASIL mutation has demonstrated that adult hippocampal neurogenesis is indeed affected[22]. We have shown that neural cell proliferation and survival are reduced in the CADASIL mice at 12 months of age. This suggests functional consequences of the impaired neurogenesis on hippocampus-dependent learning and memory functions in the model and raises the question of whether physiological neurogenic stimuli might reverse the effect of the altered Notch3.

In the present study, we further elucidate how the short-term and long-term survival of newly generated neurons in the SGZ is regulated by Notch3, and how it depends on an intact Notch3 expression (Fig. 1). Adult neurogenesis can be robustly stimulated by physical exercise[23] and environmental enrichment[24]. To investigate whether a dysregulated hippocampal neurogenesis can also be improved in CADASIL by these physiological neurogenic stimuli, female adult mice were housed in standard (STD), environmentally enriched (ENR) or running wheel cages (RUN) for either 28 days (short-term) or 6 months (long-term) (Fig. 1). To address these questions, the well-established transgenic mouse model overexpressing Notch3 with a CADASIL-causing point mutation ($TgN3^{R169C}$) was used. To control for the effects of Notch3-overexpression in itself, mice overexpressing wild type Notch3 ($TgN3^{WT}$), generated by the same approach as $TgN3^{R169C}$, were used[25].

Results

Notch3 overexpression results in reduced survival of newborn neurons after 6 months. In the long-term group, the noticeable but non-significant interaction of genotype and cage condition revealed that $TgN3^{WT}$ mice displayed reduced BrdU+/NeuN+ cell numbers (Fig. 2f) under STD compared to WT and CADASIL mice ($F(4,53) = 2.415$, $p = 0.06$; post-hoc: $TgN3^{WT}$ vs. WT, $p < 0.01$, $TgN3^{WT}$ vs. $TgN3^{R169C}$, $p < 0.05$). Such reduction in BrdU+/NeuN+ cell numbers under STD was not found in CADASIL mice ($TgN3^{R169C}$ vs. WT, $p > 0.05$).

There were no changes in the number of neuronal cells in the short-term group in either transgenic mouse line under STD cage condition (WT vs. $TgN3^{WT}$ and $TgN3^{R169C}$, $p > 0.05$).

Astrogliosis in CADASIL mice depends on the duration of cell survival. In the long-term group, CADASIL mice showed an increased percentage of newly generated BrdU+ cells differentiating into astrocytic S100β+ cells ($F(2,59) = 4.030$, $p < 0.05$; post-hoc: $TgN3^{R169C}$ vs. WT, $p < 0.05$) (Fig. 3b). This was not seen in Notch3 overexpressing mice ($TgN3^{WT}$ vs. WT, $p > 0.05$).

Astrogliosis did not occur in the short-term cell survival group in either transgenic mouse line ($F(2,66) = 1.264$, $p > 0.05$).

Representative images of the triple fluorescent staining for BrdU, S100β and NeuN are given in Fig. 4(a–h), exemplarily showing a co-labeled BrdU+/S100β+ cell (Fig. 4h) in the DG. Co-labeled BrdU+/NeuN+ cells are also presented (Fig. 4g).

Neurogenic stimulation by short-term RUN or ENR is impaired in both Notch3 overexpressing and CADASIL mice. The significant interaction of both genotype and cage condition revealed that 28 days of RUN and ENR increased the number of BrdU+ cells (Fig. 2a) only in WT mice ($F(4,60) = 4.495$, $p < 0.01$; post-hoc: STD vs. RUN and ENR, $p < 0.001$) but not in in $TgN3^{WT}$ or $TgN3^{R169C}$ mice. Further cell characterization showed that this increase was due to an enhanced survival of BrdU+/S100β+ cells ($F(4,60) = 6.037$, $p < 0.001$; post-hoc: STD vs. RUN, $p < 0.001$) (Fig. 2c) and particularly of BrdU+/NeuN+ cells ($F(4,60) = 4.147$, $p < 0.01$; post-hoc: STD vs. RUN and ENR, $p < 0.001$) (Fig. 2e).

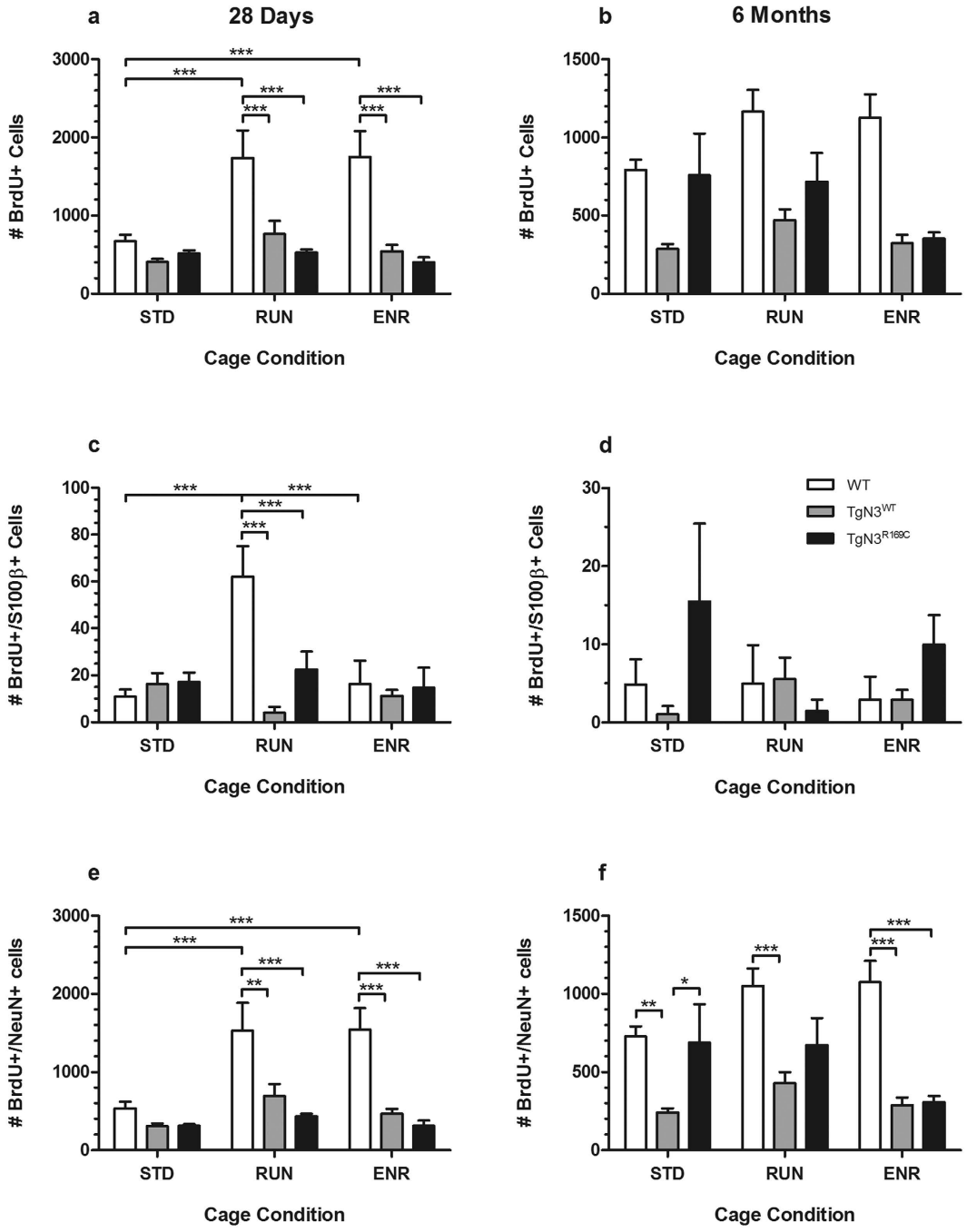

Figure 2. Results of the histological analysis of adult hippocampal neurogenesis in brain sections from WT, $TgN3^{WT}$ and $TgN3^{R169C}$ mice after 28 days (**a**,**c** and **e**) or 6 months (**b**,**d** and **f**) under standard (STD), running wheel (RUN) or environmentally enriched (ENR) cage conditions. The absolute number of BrdU+ (**a** and **b**), BrdU+/S100β+ (**c** and **d**) and BrdU+/NeuN+ cells (**e** and **f**) was quantified to determine the survival rate of proliferating cells, new astrocytic and new neuronal cells. New neuron survival is reduced in older (**f**) but not younger $TgN3^{WT}$ mice (**e**). Neurogenic stimulation by RUN or ENR failed in both $TgN3^{WT}$ and $TgN3^{R169C}$ independent of the duration (**e** and **f**). Data are expressed as mean ± S.E.M. $^{*}p < 0.05$, $^{**}p < 0.01$, $^{***}p < 0.001$.

No such increase of (neuronal) cell numbers was found after 6 months of RUN or ENR (BrdU+ cells: $F(4,53) = 2.108$, $p > 0.05$; BrdU+/NeuN+ cells: $F(4,53) = 2.415$, $p > 0.05$) either in WT or transgenic mice (STD vs. RUN or ENR: $p > 0.05$).

Representative microscope images of the BrdU staining are given in Fig. 5, demonstrating that WT mice display more BrdU+ cells after 28 days of RUN (Fig. 5d) and ENR (Fig. 5g) compared to STD (Fig. 5a). Figure 5 also shows that RUN and ENR did not stimulate BrdU+ cell survival in $TgN3^{WT}$ (Fig. 5b,e and h) or $TgN3^{R169C}$ mice (Fig. 5c,f and i).

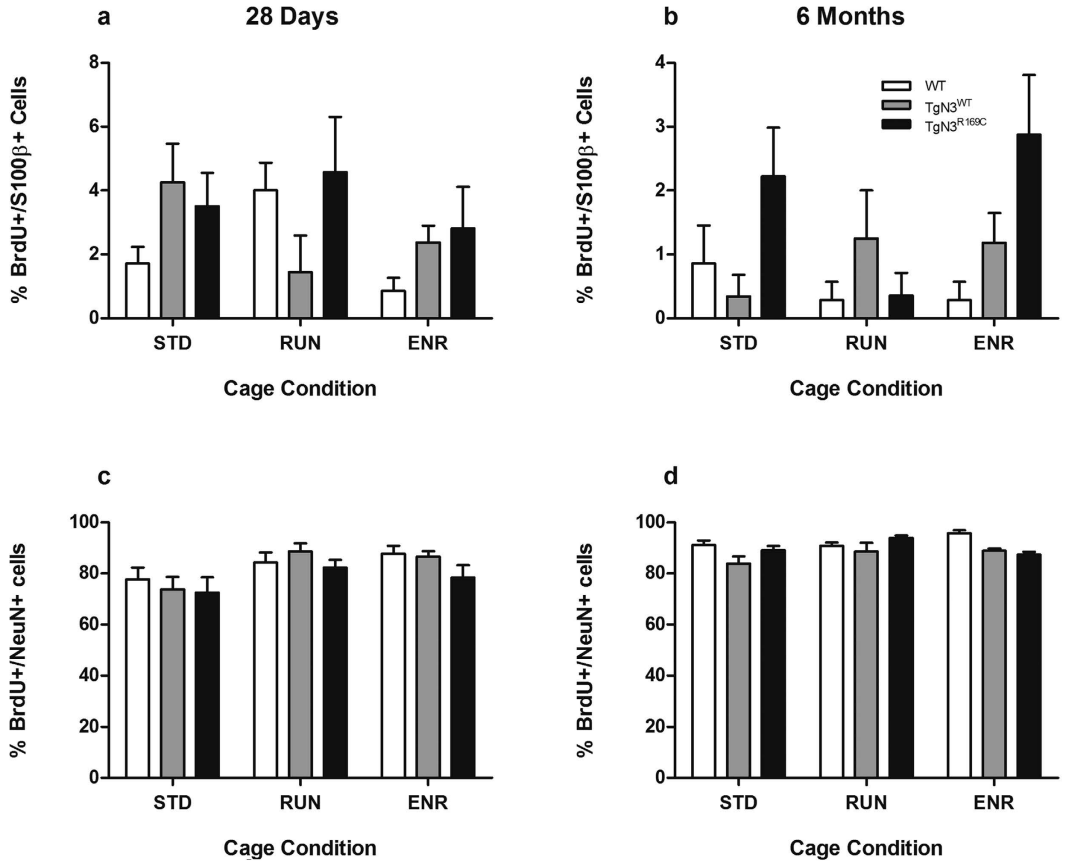

Figure 3. Results of the histological analysis of adult hippocampal neurogenesis in brain sections from WT, $TgN3^{WT}$ and $TgN3^{R169C}$ mice after 28 days (**a** and **c**) or 6 months (**b** and **d**) under standard (STD), running wheel (RUN) or environmentally enriched (ENR) cage conditions. The percentage of BrdU+/S100β+ (**a** and **b**) and BrdU+/NeuN+ cells (**c** and **d**) of all BrdU+ cells was determined to assess effects on the differentiation of BrdU+ cells to astrocytes and neurons. The percentage of BrdU+/S100β+ cells in $TgN3^{R169C}$ is increased in older mice independent of RUN or ENR (**b**). Data are expressed as mean ± S.E.M.

Running wheel activity is reduced in CADASIL mice and age-dependently decreased in Notch3 overexpressing mice. During 28 days (Fig. 6a), $TgN3^{WT}$ mice showed increased running wheel activity per 24 h compared to WT and CADASIL mice ($F(2,543) = 84.66$, $p < 0.001$; post-hoc: $TgN3^{WT}$ vs. WT and $TgN3^{R169C}$, $p < 0.001$). $TgN3^{R169C}$ mice in turn ran a shorter distance per 24 h than WT ($p < 0.001$).

During 6 months (Fig. 6b), in contrast, running wheel activity was reduced in transgenic mice ($F(2,1569) = 229.7$, $p < 0.001$; post hoc: $TgN3^{WT}$ and $TgN3^{R169C}$ vs. WT, $p < 0.001$) with $TgN3^{R169C}$ mice running even less than $TgN3^{WT}$ mice ($p < 0.001$). Detailed analysis of running wheel activity over six months (Fig. 6c) revealed that the distance run per month decreased over time in $TgN3^{R169C}$ mice ($F(5,8) = 8.121$, $p < 0.01$).

When considering just the first five days of RUN (Fig. 6d), which are most relevant for the stimulation of neural cell proliferation in the DG, WT and $TgN3^{WT}$ mice covered similar distances, while $TgN3^{R169C}$ mice showed significantly reduced physical activity per 24 h compared to WT and $TgN3^{WT}$ mice ($F(2,92) = 22.34$, $p < 0.001$; post-hoc: $p < 0.001$).

Motor coordination on the Rotarod is impaired in both transgenic mouse lines. $TgN3^{WT}$ and $TgN3^{R169C}$ mice spent significantly less time on the rotating rod than WT mice ($F(2,16) = 6.309$, $p < 0.01$; post-hoc: $p < 0.05$) (Fig. 6e). This indicates motor deficits in both transgenic mouse lines.

Discussion

The present study aimed to investigate whether adult hippocampal neurogenesis in CADASIL can be influenced in short- and long-term by physiological stimuli, which have been shown to robustly enhance it in healthy animals and neuropathological disease models[26–29]. We found that the long-term survival of new neurons was reduced in Notch3 overexpressing but not CADASIL mice under STD cage conditions compared to WT. Moreover, short- and long-term neurogenic stimulation by RUN or ENR apparently failed in both transgenic mouse lines.

The decreased neurogenesis in Notch3 overexpressing mice of the long-term group replicates the finding of our previous study in six-months-old $TgN3^{WT}$ mice[22]. The fact that the decreased neurogenesis already observed four weeks after BrdU cell labeling[22] is still evident after five more months, shows that this is really due to a suppression of cell proliferation by Notch3 overexpression, as suggested in our previous work, rather than an influence on cell

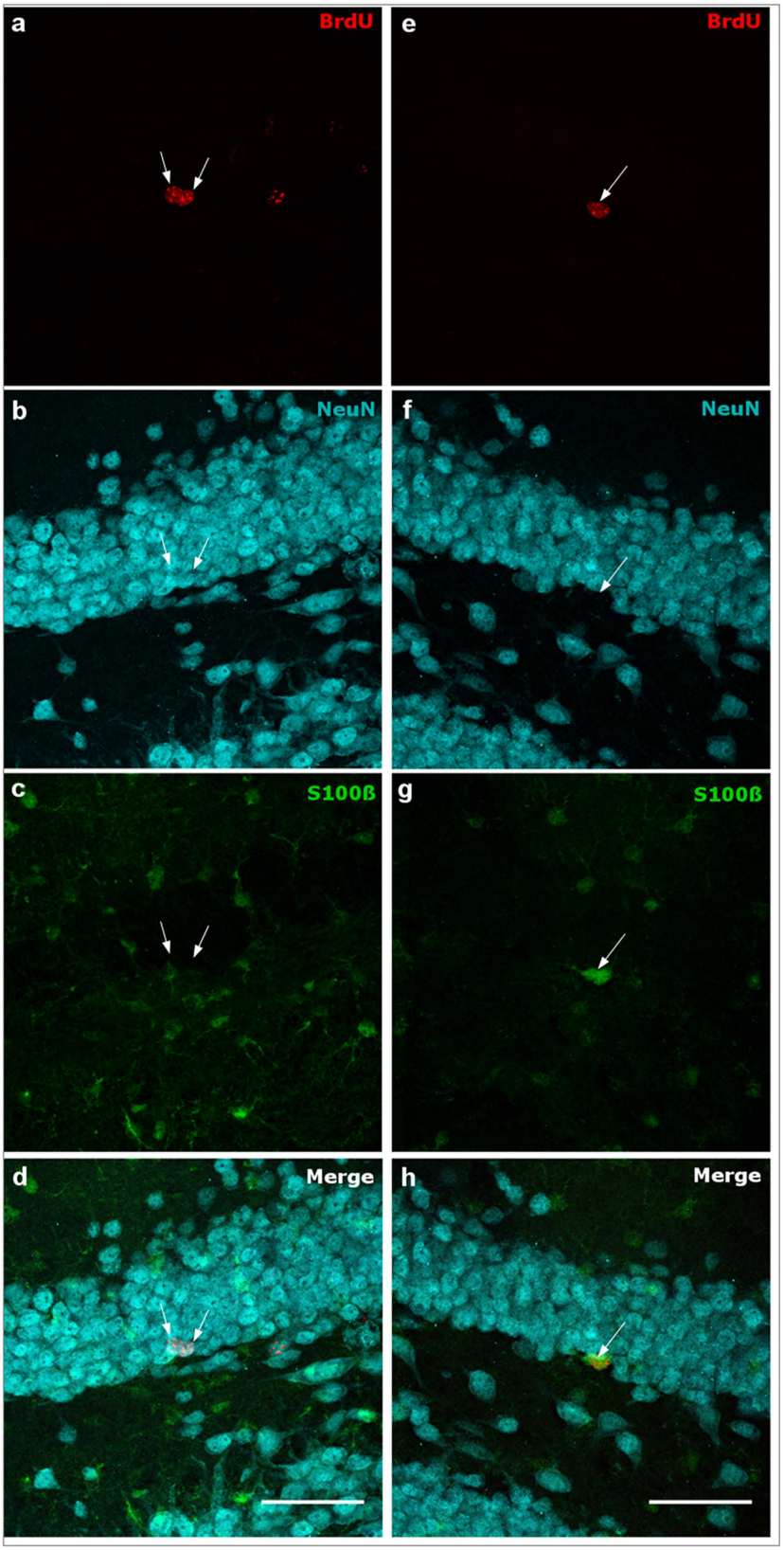

Figure 4. Representative confocal images of the triple fluorescent staining of the DG of two different mice (**a**–**d**): TgN3^{WT} ENR 6 months; (**e**–**h**) TgN3^{WT} STD 28 days). Arrows point to BrdU+ cell nuclei (red, **a** and **e**), NeuN+ cell nuclei (cyan, **b** and **f**), S100β+ cells (green, **c** and **g**), two BrdU+/NeuN+ cell nuclei (**d**) and a BrdU+/S100β+ cell (**h**). Scale bar = 50 μm.

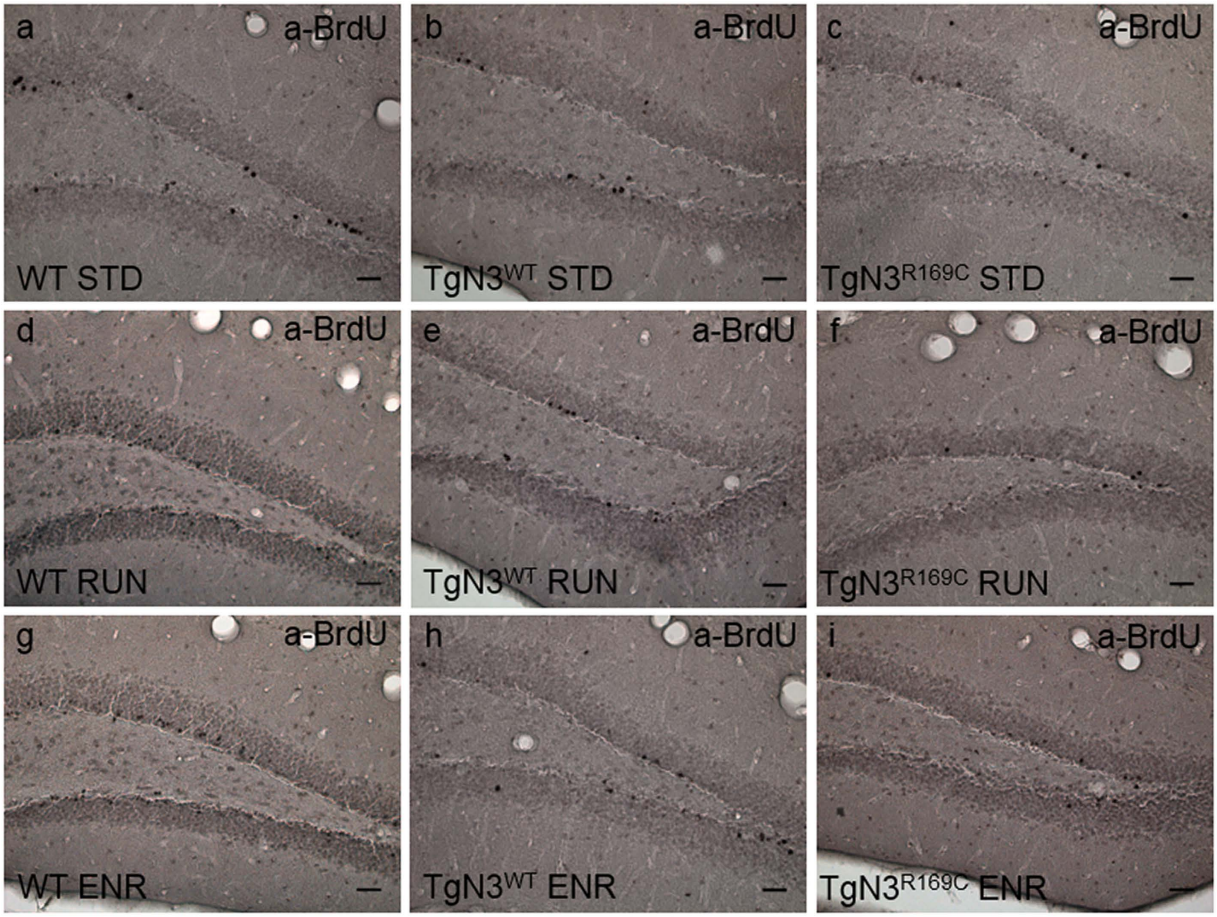

Figure 5. Representative light microscope images of the BrdU staining of the DG of each genotype after 28 days of STD (**a**–**c**), RUN (**d**–**f**) and ENR (**g**–**i**) cage conditions. They illustrate the increase in the number of BrdU-positive cells (black dots) in healthy WT animals after RUN (**d**) or ENR (**g**) and the missing stimulating effect on cell survival in Notch3 overexpressing ($TgN3^{WT}$) and CADASIL mice ($TgN3^{R169C}$). Scale bar = 100 μm.

survival. Notch3 and Notch1 are possibly co-expressed in proliferating hippocampal precursor cells[22]. Moreover, Notch1 has been shown to be essential for progenitor pool maintenance and regulation of proliferation[16,18,30]. Therefore, it can be assumed that the suppression of cell proliferation by Notch3 is usually counteracted by Notch1-activated cell proliferation leading to a balanced cell proliferation rate. Overexpression of Notch3 clearly shifts the balance towards a down-regulation of precursor cell proliferation. Surprisingly, neurogenesis is not suppressed in $TgN3^{WT}$ mice under short-term STD conditions. This might indicate an age-dependency of Notch3-dependent suppression of hippocampal neurogenesis with a counteracting mechanism being effective in younger mice of the short-term group but being lost during ageing in the long-term group.

In CADASIL mice, neurogenesis is not decreased as in Notch3 overexpressing mice. However, more newly generated cells differentiate into astrocytic cells in the long-term than in WT mice. As astrocytes are critical for neurogenesis and the neuronal long-term survival[31], an increase in their portion here could represent a counteracting mechanism for a disturbed neurogenesis due to mutated and imbalanced Notch3. In support of this hypothesis, we also found an increased amount of astrocytic cells in WT animals induced by short-term RUN, which is similar to our previous findings showing different stimuli selectively affecting distinct subpopulation of newly generated hippocampal cells[32]. This may point towards the need for an intact microenvironment in the DG for a functional neurogenesis, as the generation of astrocytes is enhanced by RUN in parallel to neurogenesis.

Usually, RUN and ENR of short- or long-term durations are robust neurogenic stimulants in healthy or aged animals[33,34] and in various rodent models of neuropathological diseases such as Alzheimer's[29] and Parkinson's disease[26]. Here, RUN and ENR cage conditions increased hippocampal neurogenesis in healthy WT mice as expected. Although Notch3 overexpressing mice of the short-term group ran more in the running wheel than WT mice, despite a reduced motor coordination tested on the Rotarod, neurogenesis remains unaffected. This suggests that although neurogenesis is not yet reduced in younger $TgN3^{WT}$ mice, it is already disturbed due to Notch3 overexpression as it could not be stimulated by RUN and ENR. In support of this, we have demonstrated in our previous work using a KCl-activation neurosphere assay that the proliferative activity of neural precursor cells was potentially reduced by Notch3 overexpression[22]. This might have prevented the activation by RUN or ENR. In contrast to the present results, Ables and colleagues[35] have been able to restore neurogenesis by RUN in a Notch1 knock-out mouse. Knock-out of Notch1 specifically diminished the undifferentiated cell pool in the SGZ

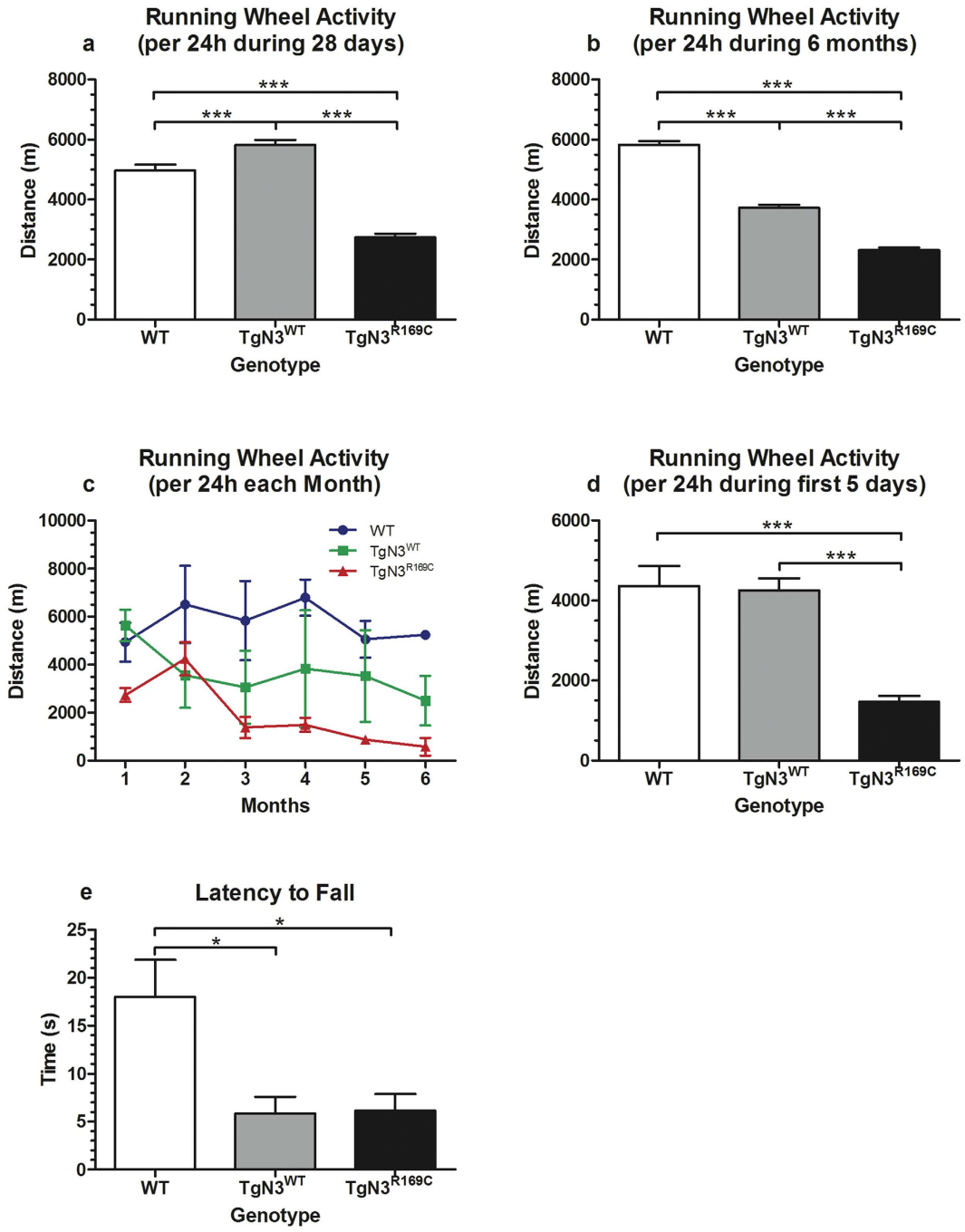

Figure 6. Effects of Notch3 overexpression ($TgN3^{WT}$) and CADASIL ($TgN3^{R169C}$) on physical activity per 24 h during 28 days (**a**), six months (**b** and **c**), during the first five days (**d**) under running wheel cage condition (RUN) and on Rotarod performance in transgenic mice corresponding to the 28 days group (**e**). Running wheel activity is reduced in $TgN3^{R169C}$ mice and duration-dependently decreased in $TgN3^{WT}$ mice (**a**–**d**). Motor coordination on the Rotarod is impaired in both transgenic mouse lines (**e**). Results of pairwise comparisons following a significant one-way ANOVA are displayed in the graphs. Data are expressed as mean ± S.E.M. $^{*}p < 0.05$, $^{***}p < 0.001$.

causing a decreased neurogenesis. RUN rescued the number of differentiated but not undifferentiated cells, indicating that this neurogenesis stimulation might not be mediated by Notch1. To clarify, if Notch3 may be involved instead, as suggested by the present results, a similar knock-out model but for Notch3 or a Notch3 antagonist[36] could be used in follow-up studies.

In CADASIL mice, hippocampal neurogenesis was similarly not increased by RUN or ENR. In contrast to Notch3 overexpressing mice, CADASIL mice showed reduced physical activity in the running wheels throughout both durations. Motor coordination on the Rotarod was also impaired. This might be interpreted as the level of physical activity in RUN, and probably also in ENR, being insufficient to stimulate neurogenesis under this

neuropathological condition. However, running wheel activity of less than 2000 m covered distance per day during 6 months has been shown to enhance neurogenesis[33]. In the present study, CADASIL mice ran mostly more than 2000 m per 24 h. Therefore, we suggest that the overexpression of mutated Notch3 disturbed the micromilieu of hippocampal precursor cells, which may have prevented these cells from reacting to RUN or ENR. This implies that not only functional Notch3 is crucial for the regulation of hippocampal neurogenesis but also its available amount in precursor cells itself and in the vascular neurogenic niche. This is of particular importance from a therapeutic point of view as it suggests that in CADASIL mutated Notch3 not only needs to be replaced but also the balance needs to be maintained.

Similar to CADASIL mice, Notch3 overexpressing mice also showed reduced physical activity (>2000 m distance covered) in the long-term and no stimulation of neurogenesis by RUN or ENR. But as they ran even more than WT mice in the short-term with still no change in neurogenesis levels, physical activity may not function as an adequate supportive therapy unless the amount of (functional) Notch3 is regulated at the same time. In ENR, however, physical activity is only one stimulation aside from visual, social and olfactory interaction with numerous other mice in a diversified equipped large cage. As the neurogenic stimulation by ENR was impaired to the same extent as by RUN, other functions than solely physical fitness could have been affected by mutated Notch3. Possible candidates are motivation, curiosity or anxiety, all of which might have been reduced in the transgenic mice, thus preventing the full experience of and benefit from ENR. This needs to be further investigated in these transgenic mouse lines.

In summary, we found that adult hippocampal neurogenesis *per se* is not altered in mice of the short-term group overexpressing wild type Notch3 or Notch3 with a CADASIL mutation. However, neurogenesis could not be stimulated by RUN or ENR of either duration, which may indicate a disturbed neurogenic process that is not reflected on the basal neurogenesis level. Considering this can be observed while no deficits in microcirculation or the vascular network have been reported[22,25], it suggests an additional independent role of Notch3 in hippocampal function. We conclude that cell intrinsic deficits in Notch3 signaling contributing to changes in adult hippocampal neurogenesis by changing the micromilieu is one vascular-independent mechanism in CADASIL patients, which might be a supporting factor for the development of cognitive deficits.

Methods

Animals. Two different transgenic mouse lines were used in this experiment. TgN3^{R169C} mice carry the R169C point mutation at exon 4 of the *notch3* gene that causes cardinal pathological features of CADASIL[25]. TgN3^{WT} mice express wild type Notch3[25]. Both transgenic lines show a 4-fold overexpression of either the mutated or the wild type Notch3 transcript and protein[25]. The FVB/N background strain served as control. FVB/N mice were obtained from Janvier Labs (Le Genest-Saint-Isle, France). Transgenic mice were bred in the Research Institutes for Experimental Medicine of the Charité Berlin (FEM). All experiments were approved by the local animal ethics committee (Landesamt für Gesundheit und Soziales, Berlin) and were carried out in accordance with the European Communities Council Directive of 22 September 2010 (10/63/EU). The genotype was confirmed by PCR following tail biopsies (Primers: Notch3 forward: 5′ TTC AGTGGTGGCGGGCGTC 3′; Notch3 reverse: 5′ GCCTACAGGTGCCACCATTA CGGC 3′; Vector forward: 5′ AACAGGAAGAATCGCAACGTTAAT 3′; Vector reverse: 5′ AATGCA GCGA TCAACGCCTTCTC 3′). To minimalize stress and conflicts in the experimental groups, only females were included in the experiments. Water and rodent lab chow were provided *ad libitum* and a constant twelve hours light/dark cycle was applied.

Experimental design. 131 eight to twelve week-old female FVB/N (WT), TgN3^{R169C} and TgN3^{WT} mice were each separated into three different cage conditions (Fig. 1). Mice maintained under standard conditions (STD) were housed in conventional cages (Makrolon cages, 0.27 m × 0.15 m × 0.42 m) in groups of two to five animals per cage. Mice kept in an enriched environment (ENR) were housed in groups of five to ten animals in larger cages (0.74 m × 0.3 m × 0.74 m), containing multiple plastic tubes, which varied in size and shape and were frequently rearranged, a cardbox house and a plastic house. In the third cage condition (RUN) mice were maintained in conventional cages in groups of two animals and provided with a running wheel (Tecniplast, Italy). Wheel turns were automatically recorded by LCD counters to monitor running wheel activity. Animals were kept in their specific cage condition either for a short (28 days) or a long (6 months) duration (Fig. 1). At the beginning of exposure to their specific cage condition, mice received three intraperitoneal (i.p.) injections of the mitotic marker Bromodeoxyuridine (BrdU, Sigma–Aldrich, Steinheim, Germany; 50 mg/kg in 0.9% NaCl) separated by an interval of 4 hours to label proliferating cells (Kuhn and Cooper-Kuhn, 2007) for the evaluation of their short- and long-term survival under the influence of wild type and mutated NOTCH3 overexpression as well as RUN and ENR.

A separate set of 20 eight to twelve week-old FVB/N, TgN3^{R169C} and TgN3^{WT} mice was exposed to the STD cage condition for 28 days and then tested on the Rotarod to assess motor coordination skills (Fig. 1)[37].

Rotarod. To test aspects of motor coordination, animals had to complete three consecutive trials on one day on the Rotarod (Columbus instruments, Columbus, OH, USA). The Rotarod consists of an elevated rod with modifiable rotating speed. Each mouse was placed on the rotating rod at a start speed of 5 rpm. When the animal found balance, the trial was started and the rod accelerated with a defined speed to a maximum of 65 rpm. The duration the animal could hold itself on the rotating rod was recorded automatically.

Perfusion and Tissue Processing. All animals were killed at the end of the experiment. First, the mice were deeply anesthetized with Ketamine/Xylazine (10% Ketamine hydrochloride, WDT; 2% Rompun, Provet AG; i.p. injection) and then transcardially perfused using 0.1 M phosphate buffered saline (PBS) followed by 4% paraformaldehyde in PBS. Brains were removed and post-fixed overnight in PFA at 4 °C and afterwards transferred

into 30% sucrose for 48 h for dehydration. Brains were then frozen in 2-methyl butane cooled with liquid nitrogen, and cut into 40 μm thick coronal sections (Bregma −0.22 mm to −3.80) using a cryostat (Leica CM 1850 UV).

Immunohistochemistry and immunofluorescence. Adult hippocampal neurogenesis was evaluated by quantifying the number of proliferating cells, which were characterized by the incorporation of BrdU. Therefore, a one-in-six series of free-floating brain sections of each animal was pretreated with H_2O_2 and HCl and then incubated with a primary anti-rat BrdU antibody (AbD serotec, 1:500) overnight at 4 °C. The next day, the sections were incubated with a biotinylated secondary antibody (Dianova, 1:125), followed by streptavidin peroxidase complex (Vectastain Elite ABC Kit, Vector Laboratories). Antibodies were visualized by diamoniobenzidine (DAB)-nickel staining, after which the brain sections were mounted on microscope slides and coverslipped.

For a more detailed investigation of neuronal and astrocytic cell types, a triple fluorescent staining against BrdU, the specific endogenous marker for Neuronal Nuclei (NeuN) and the specific marker for mature astrocytes S100β was performed. Therefore, a one-in-six series of free-floating brain sections of each animal was pretreated with HCl, followed by an overnight incubation at 4 °C with primary rat anti-BrdU antibody (AbD serotec, 1:500), mouse anti-NeuN (Millipore, 1:1000) and rabbit anti-S100β (Abcam, 1:150). The next day, sections were incubated with fluorescent secondary antibodies RhodamineX (Dianova, anti-rat, 1:250), Alexa 647 (Dianova, anti-mouse, 1:300) and Alexa 488 (Invitrogen, anti-rabbit, 1:1000) for four hours. Finally, brain sections were mounted on microscope slides and coverslipped.

Cell Quantification and image processing. For every animal, BrdU-positive (BrdU+) cells in the DAB staining were counted in nine sections containing the dentate gyrus (DG) with the SGZ, using a light microscope (Axioskop HB50/AC, Zeiss, Germany) and the 40× objective. Representative images of BrdU+ cells in the DG were taken using the 20× objective (Leica DMI 3000 B, bright field) and are shown in Fig. 5(a–i).

To detect fluorescently co-labeled BrdU/NeuN-positive (BrdU+/NeuN+) and BrdU/S100β-positive (BrdU+/S100β+) cells, 50 BrdU+ cells spread across the rostrocaudal extent of the DG were sequentially scanned (z-stacks) using a confocal microscope (Leica DM 2500). The obtained ratio was used to determine the absolute cell number. Representative confocal images of the triple fluorescent staining are shown in Fig. 4(a–h). The confocal images were taken using the 40x oil immersion objective. To get a whole image of the examined cells, 19 sequentially taken images were z-stacked. The distance between the images was 0.34 μm. Fiji for Windows 32 was used to adjust brightness and contrast.

Statistical analysis. The data sets of the short- and long-term group were graphically presented using GraphPad Prism 5 and separately analyzed using IBM SPSS Statistics 23. A two-way ANOVA was applied to analyze the effects of the investigated factors genotype and cage condition and their interaction on the numbers and percentages of BrdU+, BrdU+/NeuN+ and BrdU+/S100β+ cells. Running wheel activity during the short-term (28 days) and long-term (6 months) exercise intervention and Rotarod performance were analyzed by a one-way ANOVA. In case of a significant ANOVA, pairwise comparison using the Bonferroni post-hoc test was performed. The level of significance was set at $p \leq 0.05$.

References

1. Joutel, A. *et al.* Notch3 mutations in CADASIL, a hereditary adult-onset condition causing stroke and dementia. *Nature* **383,** 707–710 (1996).
2. Dichgans, M. Genetics of ischaemic stroke. *Lancet Neurol* **6,** 149–161 (2007).
3. Chabriat, H., Joutel, A., Dichgans, M., Tournier-Lasserve, E. & Bousser, M. G. *Cadasil. Lancet Neurol.* **8,** 643–653 (2009).
4. Joutel, A. *et al.* The ectodomain of the Notch3 receptor accumulates within the cerebrovasculature of CADASIL patients. *J. Clin. Invest.* **105,** 597–605 (2000).
5. Domenga, V. *et al.* Notch3 is required for arterial identity and maturation of vascular smooth muscle cells. *Genes Dev.* **18,** 2730–2735 (2004).
6. Craggs, L. J. *et al.* White matter pathology and disconnection in the frontal lobe in cerebral autosomal dominant arteriopathy with subcortical infarcts and leukoencephalopathy (CADASIL). *Neuropathol. Appl. Neurobiol.* **40,** 591–602 (2014).
7. Duering, M. *et al.* Strategic role of frontal white matter tracts in vascular cognitive impairment: a voxel-based lesion-symptom mapping study in CADASIL. *Brain* **134,** 2366–2375 (2011).
8. Taillia, H. *et al.* Cognitive alterations in non-demented CADASIL patients. *Cerebrovasc. Dis.* **8,** 97–101 (1998).
9. Amberla, K. *et al.* Insidious cognitive decline in CADASIL. *Stroke* **35,** 1598–1602 (2004).
10. Irvin, D. K., Zurcher, S. D., Nguyen, T., Weinmaster, G. & Kornblum, H. I. Expression patterns of Notch1, Notch2, and Notch3 suggest multiple functional roles for the Notch-DSL signaling system during brain development. *J. Comp. Neurol.* **436,** 167–181 (2001).
11. Van Praag, H. *et al.* Functional neurogenesis in the adult hippocampus. *Nature* **415,** 1030–1034 (2002).
12. Kempermann, G., Jessberger, S., Steiner, B. & Kronenberg, G. Milestones of neuronal development in the adult hippocampus. *Trends Neurosci.* **27,** 447–452 (2004).
13. Garthe, A., Behr, J. & Kempermann, G. Adult-generated hippocampal neurons allow the flexible use of spatially precise learning strategies. *PLoS ONE* **4,** e5464 (2009).
14. Kempermann, G. New neurons for 'survival of the fittest'. *Nat. Rev. Neurosci.* **13,** 727–736 (2012).
15. Spalding, K. L. *et al.* Dynamics of hippocampal neurogenesis in adult humans. *Cell* **153,** 1219–1227 (2013).
16. Breunig, J. J., Silbereis, J., Vaccarino, F. M., Sestan, N. & Rakic, P. Notch regulates cell fate and dendrite morphology of newborn neurons in the postnatal dentate gyrus. *Proc. Natl. Acad. Sci. USA* **104,** 20558–20563 (2007).
17. Hellstrom, M., Phng, L. K. & Gerhardt, H. VEGF and Notch signaling: the yin and yang of angiogenic sprouting. *Cell. Adhes. Migr.* **1,** 133–136 (2007).
18. Lugert, S. *et al.* Quiescent and active hippocampal neural stem cells with distinct morphologies respond selectively to physiological and pathological stimuli and aging. *Cell Stem Cell* **6,** 445–456 (2010).
19. Palmer, T. D., Willhoite, A. R. & Gage, F. H. Vascular niche for adult hippocampal neurogenesis. *J. Comp. Neurol.* **425,** 479–494 (2000).

20. Chabriat, H. *et al.* Cerebral hemodynamics in CADASIL before and after acetazolamide challenge assessed with MRI bolus tracking. *Stroke* **31,** 1904–1912 (2000).
21. Miao, Q. *et al.* Fibrosis and stenosis of the long penetrating cerebral arteries: the cause of the white matter pathology in cerebral autosomal dominant arteriopathy with subcortical infarcts and leukoencephaolopathy. *Brain Pathol.* **14,** 358–364 (2004).
22. Ehret, F. *et al.* Mouse model of CADASIL reveals novel insights into Notch3 function in adult hippocampal neurogenesis. *Neurobiol. Dis*. **75,** 131–141 (2015).
23. Van Praag, H., Kempermann, G. & Gage, F. H. Running increases cell proliferation and neurogenesis in the adult mouse dentate gyrus. *Nat. Neurosci.* **2,** 266–270 (1999).
24. Kempermann, G., Kuhn, H. G. & Gage, F. H. More hippocampal neurons in adult mice living in an enriched environment. *Nature* **386,** 493–495 (1997).
25. Joutel, A. *et al.* Cerebrovascular dysfunction and microcirculation rarefaction precede white matter lesions in a mouse genetic model of cerebral ischemic small vessel disease. *J. Clin. Invest.* **120,** 433–445 (2010).
26. Klein, C. *et al.* Physical exercise counteracts MPTP-induced changes in neural precursor cell proliferation in the hippocampus and restores spatial learning but not memory performance in the water maze. *Behav. Brain Res*. **307,** 227–238 (2016a).
27. Klein, C. *et al.* Exercise prevents high-fat diet-induced impairment of flexible memory expression in the water maze and modulates adult hippocampal neurogenesis in mice. *Neurobiol. Learn. Mem*. **131,** 26–35 (2016b).
28. Iggena, D. *et al.* Only watching others making their experiences is insufficient to enhance adult neurogenesis and water maze performance in mice. *Sci. Rep*. **5,** 14141 (2015).
29. Wolf, S. A. *et al.* Cognitive and physical activity differently modulate disease progression in the amyloid precursor protein (APP)-23 model of Alzheimer's disease. *Biol. Psychiatry* **60,** 1314–1323 (2006).
30. Stump, G. *et al.* Notch1 and its ligands Delta-like and Jagged are expressed and active in distinct cell populations in the postnatal mouse brain. *Mech. Dev*. **114,** 153–159 (2002).
31. Seki, T. Microenvironmental elements supporting adult hippocampal neurogenesis. *Anat. Sci. Int*. **78,** 69–78 (2003).
32. Steiner, B. *et al.* Differential regulation of gliogenesis in the context of adult hippocampal neurogenesis in mice. *Glia* **46,** 41–52 (2004).
33. Kronenberg, G. *et al.* Physical exercise prevents age-related decline in precursor cell activity in the mouse dentate gyrus. *Neurobiol. Aging* **27,** 1505–1513 (2006).
34. Kempermann, G., Gast, D. & Gage, F. H. Neuroplasticity in old age: sustained fivefold induction of hippocampal neurogenesis by long-term environmental enrichment. *Ann. Neurol.* **52,** 135–143 (2002).
35. Ables, J. L. *et al.* Notch1 is required for maintenance of the reservoir of adult hippocampal stem cells. *J. Neurosci.* **30,** 10484–10492 (2010).
36. Yen, W.-C. *et al.* Targeting Notch signaling with a Notch2/Notch3 antagonist (Tarextumab) inhibits tumor growth and decreases tumor-initiating cell frequency. *Clin. Cancer Res.* **21,** 2084–2095 (2015).
37. Karl, T., Pabst, R. & von Hörsten, S. Behavioral phenotyping of mice in pharmacological and toxicological research. *Exp. Toxicol. Pathol*. **55,** 69–83 (2003).

Acknowledgements

We thank Jennifer Altschueler and Alexander Haake for excellent technical advice and assistance. The study was funded by a grant from Else Kröner-Fresenius Foundation to B.S.

Author Contributions

C.K., A.P. and T.M. performed the animal experiments including behavioral testing. S.S., F.E.K. and P.E. accomplished the histological stainings and cell quantifications. C.K. conducted the data-analysis. C.K. and S.S. wrote the manuscript. B.S. conceived and designed the study and wrote the manuscript.

Additional Information

Competing Interests: The authors declare no competing financial interests.

How to cite this article: Klein, C. *et al.* Stimulation of adult hippocampal neurogenesis by physical exercise and enriched environment is disturbed in a CADASIL mouse model. *Sci. Rep.* **7**, 45372; doi: 10.1038/srep45372 (2017).

Publisher's note: Springer Nature remains neutral with regard to jurisdictional claims in published maps and institutional affiliations.

Curriculum Vitae

Mein Lebenslauf wird aus datenschutzrechtlichen Gründen in der elektronischen Version meiner Arbeit nicht veröffentlicht.

List of publications

Research articles	**Munder T, Pfeffer A, Schreyer S, Guo J, Braun J, Sack I, Steiner B, Klein C,** MR elastography detection of early viscoelastic response of the murine hippocampus to amyloid β accumulation and neuronal cell loss due to Alzheimer's disease. JMRI 25741, 2017. **Hain EG, Klein C, Munder T, Braun J, Riek K, Müller S, Sack I, Steiner B.** Dopaminergic neurodegeneration in the mouse is associated with decrease of viscoelasticity of substantia nigra tissue. PLoS One 11:e0161179, 2016. **Klein C, Schreyer S, Kohrs FE, Elhamoury P, A. Pfeffer A, Munder T, Steiner B.** Stimulation of adult hippocampal neurogenesis by physical exercise and enriched environment is disturbed in a CADASIL mouse model. Sci. Rep.7:45372, 2017.

Acknowledgements

During all these years, many people were of great support and this thesis would not have been possible without them. I would like to express my deep appreciation to my supervisor PD Dr. Barbara Steiner, who provided her expertise, guidance, training and time throughout the project.

Enourmous thanks to Dr. Charlotte Klein also for her assistance, tutoring and incredible knowledge.

A big shout out to my colleagues Anna Pfeffer, Stefanie Schreyer, Justyna Rasinska, Jing Guo for their continuous (professional) support und for making this time totally worthwhile. Inside the lab and outside it. In this context thanks to Anna for awesome and fruitful team work.
Also thanks to all my other friends, without you I might have never finished this thesis. Or sooner.

Finally, I would like to especially thank my father Jost, for his wisdom and advice and of course I thank my mom, Hedwig, she is the best. Also thanks to my siblings Wolf and Ina for their open ears and hearts.